Ice rafting patterns on the western Svalbard slope 74–0 ka: Interplay between ice-sheet activity, climate and ocean circulation

SIMON P. JESSEN AND TINE L. RASMUSSEN

Jessen, S. P. & Rasmussen, T. L.: Ice rafting patterns on the western Svalbard slope 74–0 ka: Interplay between ice-sheet activity, climate and ocean circulation.

The distribution of ice rafted detritus (IRD) is studied in three cores from the western Svalbard slope (1130–1880 m water depth, 76–78° N) covering the period 74–0 ka. The aim is to provide new insight in the dynamics of the Svalbard-Barents Sea Ice Sheet during Marine Isotope Stages (MIS) 4–1 to get a better understanding of ice-sheet interactions with changes in ocean circulation and climate on orbital and millennial (Dansgaard-Oeschger events of stadial-interstadial) time scales. The results show that concentration, flux, composition and grain-size of IRD vary with climate and ocean temperature on both orbital and millennial time scales. The IRD consists mainly of fragments of siltstones and mono-crystalline transparent quartz (referred to as “quartz”). IRD dominated by siltstones has a local Svalbard-Barents Sea source, while IRD dominated by quartz is from distant sources. Local siltstone-rich IRD predominates in warmer climatic phases (interstadials), while the proportion of allochthonous quartz-rich IRD increases in cold phases (glacials and stadials/Heinrich events). During the Last Glacial Maximum and early deglaciation at 24–16.1 ka, the quartz content reached up to >90%. In warm climate, local iceberg calving apparently increased and the warmer ocean surface caused faster melting. During the glacial maxima

(MIS 4 and MIS 2) and during cold stadials and Heinrich events, the local ice sheets must have been relatively stable with low ablation. During ice retreat phases of the MIS 4/3 and MIS 2/1 transitions, maxima in IRD deposition were dominated by local coarse-grained IRD. These maxima correlate with episodes of climate warming, indicating a rapid, stepwise retreat of the Svalbard-Barents Sea Ice Sheet in phase with millennial-scale climate oscillations.

Simon P. Jessen (simon.jessen@nordkapp.kommune.no), Central administration of North Cape municipality, Rådhusgata 12, PO box 403, N-9751 Honningsvåg, Norway; Tine L. Rasmussen, CAGE – Centre for Arctic Gas Hydrate, Environment and Climate, Department of Geosciences, UiT the Arctic University of Norway, Dramsveien 201, N-9037 Tromsø, Norway

The glacial climate was unstable and oscillated on millennial time scales between cold (Greenland stadial) and warm (Greenland interstadial (GIS)) climate (Bond *et al*. 1993; Dansgaard *et al*. 1993), the so-called Dansgaard-Oeschger events. Stadial-interstadial cycles were characterized by rapid changes in the activity of ice sheets, the extent and distribution of sea ice and ocean circulation in and around the North Atlantic. Icebergs and sea ice are thought to have played a significant role in modulation of past ocean circulation and climate on both orbital and suborbital time scales (e.g. Broecker *et al*. 1990; Alley & MacAyeal 1994; Gildor & Tziperman 2001; Zhang *et al*. 2014).

Sand-sized mineral grains deposited in deep-ocean hemipelagic sediments are an indication of presence of sea-ice and/or icebergs and are labeled Ice Rafted Detritus (IRD). The IRD is most often used as a proxy for ice-sheet calving activity (e.g. Ruddiman 1977; Heinrich 1988; Bond *et al*. 1993). The distribution of IRD in the central and eastern North Atlantic indicates almost synchronous calving from the Fennoscandian Ice Sheet (Fronval *et al*. 1995; Moros *et al*. 2004), the Icelandic Ice Sheet (Bond *et al*. 1992; 1993, 1997, 1999; Bond & Lotti 1995; Lackschewitz *et al*. 1998; van Kreveld *et al*. 2000) and probably also the Greenland Ice Sheet (Lackschewitz *et al*. 1998; van Kreveld *et al*. 2000) with increased calving during cold stadial phases. During the longer lasting Greenland stadials (called 'Heinrich events'), the Laurentide Ice Sheet launched armadas of icebergs into the North Atlantic. Heinrich events (H7–H1) occurred at 6–10 ka intervals during MIS 4–MIS 2 (e.g. Heinrich 1988; Broecker *et al*. 1992; Bond *et al*. 1993; Alley & MacAyeal 1994). A conceptual model based on five detailed records of IRD from the British margin showed high IRD flux during the cold stadials/Heinrich events and sharp increases in the flux during the rapid warmings to the interstadials (Scourse *et al*. 2009).

Here, we present a detailed study of the distribution and composition of IRD from the western Svalbard slope, northeastern Greenland Sea in the polar North Atlantic in centennial resolution in three core records with detailed age models (piston cores JM03-374PC, JM03-373PC2 and JM04-025PC from 1130 m, 1485 m, and 1880 m water depth, respectively). Together, the cores provide long sequences of undisturbed sediments dating back to 74 ka. We study the concentration, flux, mineral composition and grain-size of the IRD. Combined with previously published data of sedimentation rates (Rasmussen *et al*. 2007; Jessen *et al*. 2010), we investigate the calving activity of the western part of the Svalbard-Barents Sea Ice Sheet during the glacial build-up phase in early MIS 2 and during peak glaciations of the shelf in MIS 4 and late MIS 2. Further, we study the impact of changes in surface water temperature on the concentration, grain-size, mineral composition and provenance of the IRD and ice sheet activity in relation to millennial-scale climate changes from warm interstadials to cold stadials and Heinrich events. The aim is to reconstruct the activity of the Svalbard-Barents Sea Ice Sheet on orbital and millennial time scales to improve the understanding of timing and patterns of ice-sheet retreat and advance in relation to both gradual and abrupt oceanographic and climatic changes.

Physical setting

Glacial settings and potential IRD sources

Today, 60% of the Svalbard archipelago is covered by glaciers. In MIS 4 and 2, the Svalbard-Barents Sea region was fully glaciated (e.g. Hebbeln &Wefer 1997; Mangerud *et al*. 1998; Vogt *et al*. 2001). The major part of the Svalbard-Barents Sea Ice Sheet was marine-based and located on the present-day seafloor of the Barents Sea and on the shelf off Svalbard (e.g.

Siegert & Dowdeswell 2002, 2004; Lambeck 2004; Ottesen *et al*. 2005, 2007). The last peak glaciation occurred at 24 ka and the retreat of the ice sheet began shortly thereafter (e.g. Jessen *et al*. 2010 and references therein; Hormes *et al*. 2013; Patton *et al*. 2015).

The IRD deposited on the western Svalbard slope consists mainly of fragments of siltstones and mono-crystalline quartz (Goldschmidt *et al*. 1995) (hereafter referred to as “quartz”). The bedrock and most of the sediments on the seafloor of the Barents Sea consist of fine-grained sedimentary rocks (Kelly 1988). The shallow Spitsbergen Bank between Spitsbergen and Bjørnøya (Fig. 1) is a well-known local source of siltstones including black shales dating from the Jurassic (Edwards 1975; Kelly 1988; Goldschmidt *et al*. 1995; Andersen *et al*. 1996; Vogt *et al*. 2001). Thus, dark coloured siltstones including black shales are used as indicators for icebergs coming from Svalbard and the Barents Sea (Spielhagen 1991; Wagner & Henrich 1994; Andersen *et al*. 1996). Hebbeln & Wefer (1997) distinguished between three main source areas of IRD in the Fram strait: i) the Svalbard-Barents Sea Ice Sheet, ii) the Fennoscandian Ice Sheet and iii) the shelves of the Arctic Ocean.

Oceanographic setting

The western Svalbard continental slope is draped with contouritic sediments deposited by the relatively strong bottom currents flowing along the western Svalbard margin (Eiken & Hinz 1993; Howe *et al*. 2008; Rebesco *et al*. 2014). Today, Atlantic surface Water flows northward into the Arctic Ocean together with Greenland Sea Intermediate Water (Fig. 1) (Hopkins 1991). The inflow to the Arctic Ocean through the eastern part of the Fram Strait is counter-balanced by outflow of sea-ice loaded Polar surface water of the East Greenland Current together with return Atlantic water and Arctic Ocean Deep water in the western Fram Strait (e.g. Eldevik *et al*. 2009). In the northeastern Fram Strait, the Atlantic water submerges and flows into the Arctic Ocean as a warm (>2 °C) subsurface current under a cold, fresh and sea-ice covered layer of Polar surface water (<-1 °C). During the Last Glacial Maximum the circulation pattern of the western Svalbard slope was comparable to the present day, but with colder Atlantic water at the surface (Rasmussen *et al*. 2007). During the last deglaciation from North Atlantic Heinrich Event 1 and to the Early Holocene, Atlantic water flowed along the slope, but as a subsurface current below cold polar meltwater (Rasmussen *et al*. 2007; Ślubowska-Woldengen *et al*. 2007). In the Early Holocene at 10.2±0.2 ka, Atlantic water re-appeared at the surface west of Svalbard.

Material and methods

Three high-resolution piston cores were taken from the western Svalbard slope during cruises with *RV Jan Mayen* (now *RV Helmer Hanssen*) in 2003 and 2004: JM03-373PC2 (Rasmussen *et al*. 2007; Jessen *et al*. 2010), JM03-374PC (Jessen 2005), and JM04-025PC (Jessen *et al*. 2010; Jessen & Rasmussen 2015) (Fig. 1). Core JM03-373PC was taken from Storfjorden Fan at 1485 m water depth. The core contains a debris flow deposit dated to 24 ka at the bottom (Rasmussen *et al*. 2007; Jessen *et al*. 2010). Core JM03-374PC is located north of Storfjorden Fan at 1130 m water depth. This core is the most proximal to the former ice sheet on Svalbard of the three studied cores. Core JM04-025PC is located at 1880 m water depth at the lower part of the Isfjorden Fan. This core is the most ice-distal of the three investigated cores.

Wet bulk density was measured with a GEOTEK Multi Scanner Core Logger before opening of the cores (Jessen *et al*. 2010). Core JM03-373PC2 has previously been AMS ^{14}C dated and investigated for the distribution of benthic and planktic foraminiferal faunas, concentration of IRD >150 µm, stable isotope composition of shells of benthic and planktic foraminifera (Rasmussen *et al*. 2007), and IRD >500 µm (Jessen *et al*. 2010). The upper part of core JM04-025PC (30–0 ka) has been investigated for AMS ^{14}C dates, magnetic susceptibility and concentration of IRD >500 µm (Jessen *et al*. 2010). The whole core has been studied for stable isotope values and grain-size of sortable silt (Jessen & Rasmussen 2015). For core JM03-374PC, AMS ^{14}C dates have been published by Jessen *et al*. (2010) and IRD concentrations in the size fractions >150 µm, >250 µm and >500 µm and proportion of quartz grains were treated in Jessen (2005).

Samples were taken in 2 or 2.5 cm (cores JM04-025PC, JM03-374PC) or 5 cm intervals (core JM03-373PC) in 1-cm thick slices, weighed, dried and weighed again and subsequently wet sieved over mesh-sizes 63 and 100 µm (Jessen 2005; Rasmussen *et al*. 2007; Jessen *et al*. 2010). For the present study of core JM04-025PC, the residues >100 µm were dry sieved into grain-size fractions 150–250 µm, 250–500 µm, and >500 µm. The fractions 250–500 µm and >500 µm were counted on a picking tray under a binocular microscope. At least 300 grains were counted in each sample. In samples with less than ~500 grains all grains were counted. Mineral classes were determined in the size-fraction 250–500 µm. Twelve different mineral classes were quantified, but in the present study we only focus on the two dominant mineral classes, quartz and siltstones. The % quartz and % siltstones were calculated relative to total IRD content in a sample. Thereafter, the IRD of the 100–500 µm size fraction was dry sieved over a 150-µm mesh-size sieve and the IRD counted in the fraction 150–500 µm. For IRD in cores JM03-374PC and JM03-373PC2, the same procedures for counting as in core JM04-025PC were followed. IRD concentrations (no. of mineral grains/g) are given relative to dry weight. The IRD flux (no. grains cm^{-2} ka^{-1}) is calculated using: IRD counts in no. grains g^{-1} dry weight x dry bulk density (g cm^{-3}) x sedimentation rate (cm ka^{-1}).

Core JM03-373PC is presented on the age model from Jessen *et al*. (2010) re-calibrated using the calibration program Calib7.02 and the Marine13 database (Stuiver & Reimer 1993; Reimer *et al*. 2013). Data from JM03-374PC and JM03-373PC are likewise presented with re-calibrated ^{14}C ages (Table 1; see Section 'Age control'). A reservoir age correction of -405 years inherent in the calibration program was used.

Grain-size of IRD

A grain-size ratio was calculated to perform a first order quantitative measure of changes in the grain-size of the IRD. The ratio between the counts of IRD in two different grain-size fractions, >500 µm and 150–500 µm was calculated for each sample and normalized to the average of the core. The grain-size of 500 µm was chosen as the cut-off size, because IRD coarser than 500 µm is generally considered to be mainly iceberg rafted (e.g. Dowdeswell & Dowdeswell 1989; Pfirman *et al*. 1989; Hebbeln 2000). Sea ice can transport sediments of any grain-size (e.g. Bischof 2000), however, iceberg-rafted IRD is on average more coarse grained than sea-ice rafted IRD (e.g. Dowdeswell & Dowdeswell 1989):

$$\frac{\text{No. }>500\ \mu\text{m x no. }(150\text{–}500\ \mu\text{m})_{\text{sample}}{}^{-1}}{\text{No. }>500\ \mu\text{m x no. }(150\text{–}500\ \mu\text{m})_{\text{average}}{}^{-1}} \qquad (1)$$

A grain-size ratio >1 indicates a relatively coarse-grained sample with a higher proportion of coarse-grained IRD than the normal for the core, while a grain-size ratio <1 indicate a relatively fine-grained sample. A high grain-size ratio should indicate a higher proportion of iceberg-rafted IRD than the normal, and vice versa, a low grain-size ratio should indicate a high proportion of sea-ice rafted grains.

In addition, in core JM04-025PC, the grain-size of IRD is determined from end-member modelling based on the counts in the two grain-size fractions >500 µm and 150–500 µm. The counts of the two grain-size classes are plotted in a scatter-plot and a coarse-grained end-member and a fine-grained end-member is determined from the grouping of the data points (see Section 'Fine-grained versus coarse-grained IRD'). Only samples with at least 20 grains of IRD >500 µm are used to define end-members.

Results and interpretations

Age control

The age models of cores JM03-373PC and JM04-025PC have been published before in Jessen *et al*. (2010) and Jessen & Rasmussen (2015), respectively. The age models for all three cores are based on calibrated AMS ^{14}C dates, magnetic susceptibility (MS), lithology and MS tie-points 1–9 defined by Jessen *et al*. (2010) (Fig. 2; Table 1). In addition, correlation of the $\delta^{18}O$ records (Fig. 3) and the location of the Laschamps geomagnetic excursion in cores JM04-025PC and JM03-374PC is used (Snowball *et al*. 2007) (Figs 2, 3). One extra MS tie-point has been defined in all three records, MS tie-point 6.1 (Fig. 2), by a distinct decline in magnetic susceptibility correlating with a peak in concentration of IRD and a coarsening of the IRD seen as a grain-size ratio >1 (Fig. 4). The age model of JM03-373PC sets the age of the tie-point to 20.17±0.170 ka (Fig. 4; Table 1). In general, linear sedimentation rates between dating points and tie-points were assumed except between tie-points 6 and 7, where the sedimentation rate changes at *c*. 20 ka (Jessen *et al*. 2010) (Fig. 5).

After establishing the initial age model, the part of the age model older than 24 ka in core JM04-025PC has been tied to the GICC05 ice-core age scale based on the grain-size of sortable silt and the $\delta^{18}O$ record (Jessen & Rasmussen 2015) (Fig. 6). North Atlantic Heinrich events 6 and 1 (H6 and H1) that occur at isotope stage transitions MIS 2/1 and MIS 4/3, respectively are particularly well-defined in marine records (e.g. Bond *et al*. 1993). In core JM04-025PC, these two events stand out by very low $\delta^{18}O$ values in both planktic and benthic foraminifera (Rasmussen *et al*. 2007; Rasmussen & Thomsen 2013) (Fig. 3). Heinrich Events H7, H6, H5.2, H5, H4, H3, H2 and H1, stadials and Dansgard/Oeschger events are identified mainly based on the correlation between the sortable silt record and the NorthGRIP ice core $\delta^{18}O$ record together with excursions to low planktic $\delta^{18}O$ values (Jessen & Rasmussen 2015) (Figs 3, 6). The tuning was done to account for the possibility of changing sedimentation rates along with the changing climate on both orbital and millennial time scales. In this study in core JM04-025PC, we use the GICC05 age scale for the part older than 30 ka, and the re-calibrated magnetic susceptibility chronology adapted from Jessen *et al*. (2010) for the part younger than 30 ka.

Two AMS ^{14}C dates from core JM05-031GC have been transferred to JM03-374PC based on correlation of the magnetic susceptibility records and the benthic oxygen isotope records of the two cores (Figs 2, 3). By linear interpolation the age of the bottom of core JM03-374PC is calculated to *c*. 45.8 ka. The part of core JM03-374PC older than 30 ka has been graphically correlated to JM04-025PC based on magnetic susceptibility and the concentrations and grain-sizes of IRD (Fig. 6). According to this, core JM03-374PC reaches back to *c*. 47.5 ka on the GICC05 age scale. The age estimate based on the correlation to the age model of core JM04-025PC is not significantly different from the initially calculated age of 45.8 ka. Thus, core JM03-374PC is also tied to the GICC05 ice core chronology.

Distribution of IRD: General trends in concentration, size and composition

In core JM04-025PC, quartz and siltstones constitute 87% of all counted grains (Figs 7B,C, 8A). Siltstones and quartz also dominate the IRD in cores JM03-373PC and JM03-374PC (Jessen 2005). In the two glacial stages (MIS 4 and MIS 2, 74–63 ka and 30–16.1 ka, respectively), the IRD concentration is relatively high (Fig. 7A). In MIS 2 in core JM04-025PC, the IRD mainly consists of quartz, with percentages exceeding 90% (Fig. 7B) (and 70% in JM03-374PC (Jessen 2005)). Increasing IRD concentrations generally coincide with fining of the IRD (Fig. 7A,D), except at *c*. 24 ka, where IRD is abundant, coarse grained, and rich in siltstones. In MIS 4, the IRD was mainly fine-grained and less rich in quartz compared to MIS 2. Quartz is still more abundant than siltstones with the exception of two short-lived peaks in % siltstones at *c*. 69 and 64 ka (Fig. 7C,D).

In MIS 3 (60–30 ka BP), the concentration of IRD is very variable. The composition and grain-size of the IRD vary on 1–2 ka time scales (Fig. 8B,C). Between 56 and 46 ka, the IRD concentration is higher, and the IRD coarser grained and richer in siltstone fragments than between 46 and 30 ka, when the IRD is mainly fine grained, of generally lower concentration and rich in quartz (Fig. 7D).

The deglaciations (MIS 4/3 and MIS 2/1 transitions at 56–46 and 16.1-*c*. 10.2 ka, respectively) are characterized by deposition of relatively coarse-grained, often siltstone-rich IRD (Fig. 7B,D). The IRD concentration during the MIS 2/1 transition was lower than during MIS 2, but because the sedimentation rate was 3.6 to 15 times higher during the deglaciation (MIS 2/1 transition) than during MIS 2, the flux of IRD was in fact on average four times higher (Jessen *et al*. 2010). One high peak in concentration of siltstone-rich and coarse-grained IRD is seen around 61 ka in the MIS 4/3 transition interval followed by several similar peaks in early MIS 3 (56–46 ka) (Fig. 7A,C,D). Both the MIS 4/3 and MIS 2/1 transitions on the western Svalbard slope are characterized by low flux and concentrations of foraminifera, probably because of the high sedimentation rates creating difficult environmental conditions (see Rasmussen *et al*. 2007, 2014).

In the earliest Holocene, between 11.7 and 10.2 ka, the concentration and flux of IRD are high similarly to the deglaciation and with a high content of coarse-grained siltstones. A minimum in the concentration of IRD occurs in the Early Holocene (10.2–8.5 ka). Thereafter, the IRD concentration increases steadily towards the Late Holocene (Figs 4E, 7A).

IRD provenance

Evidence from mass-transport deposits. – All three cores contain mass-transport deposits dating to *c*. 24 ka (Rasmussen *et al*. 2007; Jessen *et al*. 2010) (Figs 2–5). These sediments have been in direct or close contact with the local ice sheet (e.g. Vorren *et al*. 1989; Vorren & Laberg 1997; Elverhøi *et al*. 1995). The sand grains can thus provide evidence for the composition and grain-size of locally derived material and can serve as a form of 'ground truthing' for the distinction between local IRD and IRD from elsewhere.

The mass-transported sediments in core JM04-025PC, the most ice-distal of the cores, contain more than 45% siltstones (Figs 7C, 8A). In core JM03-374PC, the ice-proximal record, the siltstone content reaches up to >80% (Jessen 2005). In JM03-373PC from Storfjorden Fan, the coarse material is dark coloured (Rasmussen *et al*. 2007; Jessen *et al*. 2010) and consists mainly of black shales. Andersen *et al*. (1996) in cores from the western Svalbard margin, found a generally higher content of "dark mudstones" in the upper slope records closer to land than on the lower slope further offshore. The content in the sediments of black shales decreases towards Greenland, which also points to that Svalbard and the Barents

Sea are the main source (Spielhagen 1991).

Local versus allochthonous IRD. – Samples from the mass-transport deposit and samples from the MIS 4/3 and MIS 2/1 transitions have high proportions of siltstones. We use the lowest observed amount of siltstones in samples of mass-transported grains, 45%, as a cut-off value for a local end-member of siltstones (Fig. 8A).

In JM04-025PC, the quartz content occasionally exceeds 90% (Fig. 8A). Even though outcrops of Lower Cretaceous sandstones with local quartz percentages exceeding 90% are found in Svalbard, the average quartz percent for these stratigraphic units is considerably lower, <70% (e.g. Maher *et al*. 2004). They are mostly located in southeastern Svalbard facing Storfjorden (e.g. Maher *et al*. 2004; Grundvåg & Olaussen 2017) (Fig. 1B). Triassic sandstones also occur in Svalbard, but with lower quartz percentages than the Cretaceous deposits. Highest quartz content is found in Triassic deposits of northern Norway (Lundschien *et al*. 2014). Thus, there is no likely large local source from Svalbard for such high quartz content and IRD with a very high content of quartz is considered allochthonous IRD. We note, that the proportion of quartz is lowest in the most ice-proximal core JM03-374PC, which except for a few peaks reaching 70%, generally remains below 50–60% quartz (Jessen 2005; see also Discussion). Quartz-rich IRD may originate from Scandinavia (e.g. Kolla *et al*. 1979; Leinen *et al*. 1986) and IRD in cores from the Vøring Plateau off western Norway are reported to consist mainly of quartz (Dahlgren & Vorren 2003). Quartz percentages above 90% in the >250 μm size fraction have been observed in records from the Arctic Ocean, where the shallow shelf of the Kara Sea area is suggested as the main source together with the small Ellef Ringnes Island north of Canada (Bischof & Darby 1997). Thus, ice entering the Fram Strait from the Arctic Ocean is a potential source for very quartz-rich IRD west of

Svalbard.

High quartz percentages are accompanied by low siltstone percentages and the allochthonous end-member is calculated from low abundance of siltstones (Fig. 8A). The cut-off value for 100% allochthonous IRD is arbitrarily set at 5% siltstones, because some fragments of siltstones are likely to originate from foreign sources. Thus, samples with ≤5% siltstones are defined as 100% allochthonous. Samples with ≥45% siltstones are defined as 100% local. The amount of allochthonous versus local IRD in samples with siltstone content between 5% and 45% are calculated as a linear mixing product of the two end-members.

Fine-grained versus coarse-grained IRD. – A scatter plot of counts of grains in the two size fractions >500 µm and 150–500 µm show two groups of samples that differ from the majority. One group of samples shows relatively high amount of IRD >500 µm relative to IRD in the size-fraction 150–500 µm, and one group of samples shows a relatively high amount of IRD 150–500 µm relative to IRD >500 µm (Fig. 8B). From these two clusters of samples, we define two end-members, a coarse-grained end-member and a fine-grained end-member. The coarse-grained end-member is calculated from the distribution of grains in samples of the mass-transport deposit, because some of these are among the coarsest material in the cores and group in the upper left part of the diagram (Fig. 8B). The fine-grained end-member is primarily determined from a cluster of data points in the lower right part of the diagram with grain-size ratio <0.5. A sample plotting on or below the fine-grained end-member is treated as 100% fine grained, samples plotting on or above the coarse-grained end-member are treated as 100% coarse grained. Samples plotting between the end-members are described as a linear mixing product of the two end-members.

A four end-member model for IRD. – By combining the two end-member models, the IRD record can be divided into four end-members (Fig. 9A): 1. Local coarse grained, 2. Local fine grained, 3. Allochthonous coarse grained, and 4. Allochthonous fine grained (Fig. 9B–E).

Discussion

Orbital scale variations in IRD deposition and activity of the Svalbard-Barents Sea Ice Sheet

Vogt *et al*. (2001) noted that the two deglaciations of the Svalbard-Barents Sea Ice Sheet at the MIS 4/3 and MIS 2/1 transitions were very similar. This is also apparent in the record of JM04-025PC with high IRD concentrations during deglaciations and high input of local coarse-grained IRD (Figs 9A,D, 10A,D). As also observed by Vogt *et al*. (2001), the glacial stages MIS 4 and MIS 2 likewise show clear similarities in the IRD content and are characterized by high input of allochthonous, fine-grained IRD (Figs 9C,D, 10C,D). Based on these and other similarities, we divide the records into three general time intervals: i) Ice-sheet advance and peak glaciations (MIS 4 and MIS 2), ii) Intervals of glacial retreat (MIS 4/3 and MIS 2/1 transitions and early MIS 3), and iii) Intervals with a small-sized ice sheet, when the Barents Sea and most of the Svalbard fjords were free or nearly free of ice (the Holocene and mid-late MIS 3). One extreme event at *c*. 24 ka with down-slope mass wasting and intense ice rafting occurs within MIS 2 (see Section 'The 24 ka event').

Ice-sheet advance and peak glaciation (including H6 and H1), 74–56 ka and c. 30–16.1 ka. – At *c*. 30 ka, a high peak in local coarse-grained IRD is seen (Fig. 9D). Earlier reconstructions of advance of the Svalbard-Barents Sea Ice Sheet indicate that it reached the coast around this time (Andersen *et al*. 1996; Mangerud *et al*. 1998). After 30 ka, a low percentage of local IRD (Fig. 10D,E) and low sedimentation rates (Jessen *et al*. 2010) point to low local calving activity or that the locally calved-off icebergs melted elsewhere. Between 24 ka and 16.1 ka local IRD was nearly absent (Figs 9D,E, 10D,E). Generally high δ^{18}O values point to very limited meltwater production from the local ice sheet (cf. Bond *et al*. 1993) (Fig. 3A,B). The presence of allochthonous, coarse-grained IRD (Fig. 9B) shows that icebergs were present and melted over the slope. Thus, the absence of local, coarse-grained IRD either reflects little local iceberg production during the ice-sheet advance or that icebergs did not reach as far as the site of JM04-025PC. In core JM03-374PC from 1130 m water depth, generally high quartz percentages with peaks of up to 60–70% also point to mainly allochthonous IRD at 24–16.1 ka (Fig. 11B). Between 28.5 and 26 ka low quartz percentages in JM03-374PC point to some deposition of local IRD, but with very low flux (Fig. 11A). In core JM03-373PC, the concentration of IRD >500 μm is continuously low at 24–16.1 ka (Fig. 4A), while the peaks in IRD >150 μm mainly consist of quartz (Jessen 2005). IRD from the three cores together point toward low local iceberg production during MIS 2. Similarly, during MIS 4 at 74–63 ka local, coarse-grained IRD is almost absent (Figs 9E, 10E) and planktic δ^{18}O values are generally high (Fig. 3B) indicating little local iceberg and meltwater production. In a core from north of Svalbard, absence of IRD, low sedimentation rates and high δ^{18}O values at *c*. 34–24 ka were taken as an indication that minimal ice loss accelerated the final glacial growth of the ice sheet (Knies *et al*. 1999). Based on numerical modelling, Hughes (1996, 2002) proposed that limited calving of icebergs was a necessity for the build-up of the Svalbard-Barents Sea Ice Sheet. Our observations of very low amounts of local, coarse-grained IRD together with high planktic δ^{18}O similarly indicate minimal ice loss, i.e. low ablation from the western margin of the Svalbard-Barents Sea Ice Sheet during MIS 2 and 4. A coarse-grained layer in core JM02-460GC/PC from Storfjorden Trough on the shelf dating to between *c*. 18.8 and 18.1 ka was probably related to a glacier re-advance (Rasmussen *et al*. 2007). This correlates in time with early H1 and a well-documented event of huge and rapid meltwater discharges from southern Norway (Hjelstuen *et al*. 2004; Lekens *et al*. 2005). In JM04-025PC, the local end-members are completely lacking at 18.7–18.1 ka and the IRD is mainly allochthonous and fine-grained (Fig. 10 C–E). In JM03-373PC, IRD in the size-fraction 150–500 μm is abundant, while IRD >500 μm is nearly absent (Fig. 4A). The IRD pattern is consistent with a stable and probably re-advancing local ice sheet not losing mass and a fresher, sea-ice covered surface water over the slope. A recent study based on in-situ ^{10}Be and ^{14}C measurements suggests a significant thinning of the outlet glaciers in Hornsund (south-western Svalbard coast) as early as 18 ka (Young *et al.* 2018). Core JM04-374PC on the slope off Hornsund shows a clear increase in flux of local coarse IRD at *c*. 18 ka (Fig. 11A–C). Local coarse IRD is also present in JM04-025PC (Figs 9C, 10D, 11A–C).

MIS 2 is the only interval with abundant allochthonous, coarse-grained IRD constituting 40–75% of the total IRD (Figs 9B, 10B). Large ice sheets were present all around the Nordic Seas and the Arctic Ocean ensuring several potential distant iceberg sources (e.g. Spielhagen 1991; Hebbeln *et al*. 1994; Svendsen *et al*. 2004; Scourse *et al*. 2009; Mangerud *et al*. 2011).

The 24 ka event (H2/GIS2): ice stream activity and rapid ice-sheet retreat. – Mass-transport deposits are interpreted as monitors for ice-stream activity at the shelf break (e.g. Laberg & Vorren 1995; Vorren & Laberg 1997; Elverhøi *et al*. 1998; Dimakis *et al*. 2000). The numerous mass-transport deposits dating to *c*. 24 ka in cores from the western Svalbard slope show that the shelf must have been fully glaciated at that time (e.g. Jessen *et al*. 2010) (Figs 2, 3). In all cores, the mass-transport deposits are overlain by a layer of local, coarse-grained IRD (Figs 2, 3, 7). The magnetic susceptibility records show that both the mass-transport deposits and the IRD layer on top have very low magnetic susceptibility values all along the western Svalbard slope (Jessen *et al*. 2010; Sztybor & Rasmussen 2017) including the Yermak Plateau, northwest Svalbard (Chauhan *et al*. 2014).

A likely explanation for major iceberg calving events is increase in activity of ice streams seen as well-preserved mega-scale glacial lineations in troughs and fjords of western Svalbard (e.g. Ottesen *et al*. 2005, 2007). Increased ice-stream flow would lead to ice-sheet thinning and intensified iceberg calving (Benneth 2003). Recent land-based investigations also indicate thinning of the west Svalbard part of the ice sheet between 26±2.3 and 20.1±1.6 ka (Gjermundsen *et al*. 2013; Hormes *et al*. 2013). Glacial retreat prior to 20 ka is indicated from core studies of the western Svalbard margin. Hemipelagic sediments in cores from troughs dating to >19 ka show that the outer part of Storfjorden and Bellsund troughs has been ice free since at least *c*. 20 ka (Cadman 1996; Rasmussen *et al*. 2007; Ślubowska-Woldengen *et al*. 2007). IRD originating from the Barents Sea shelf is found in a deep-sea core off Jan Mayen dating to between 25.3 and 23.3 ka (Bauch *et al*. 2001) (Fig. 1A), which also points to increased activity of the Svalbard-Barents Sea ice streams. Together, the evidence indicate intensified ice-stream activity at *c*. 24 ka resulting in increased ablation via iceberg calving, thinning of the ice sheet and rapid glacial retreat from the outer shelf. Remnants of the ice sheet seem to have remained between the troughs for several millennia (e.g. Landvik *et al*. 2005, 2013, 2014; Alexanderson *et al*. 2011). The timing apparently correlates with North Atlantic Heinrich Event 2 (H2) or Greenland interstadial 2. The eustatic sea level rise following Heinrich events was 10–15 m (Chappell 2002). Both a sea level rise, ocean warming or a combination of the two are possible triggers of instability of the ice sheet (e.g. Hulbe 1997; Hulbe *et al*. 2004; Shaffer *et al*. 2004; Marcott *et al*. 2011).

Intervals of glacial retreat 56–46 ka and 16.1–10.2 ka. – The two intervals of glacial retreat, the MIS 4/3 and MIS 2/1 transitions show very similar patterns in the IRD record, but differ in the duration of the events (Figs 9, 10). Both periods are characterized by episodic deposition of local, coarse-grained IRD indicating local calving and ice-sheet retreat (Figs 9D, 10D). Series of glacigenic bed shapes in the Barents Sea display a very dynamic MIS 2/1 transition with cycles of glacial still-stands and re-advances (Andreassen *et al*. 2008; Hogan *et al*. 2010; Winsborrow *et al*. 2010; Rüther *et al*. 2011; Bjarnadóttir *et al*. 2012; Nielsen & Rasmussen 2018). The most conspicuous episode of the deglaciation was probably at *c*. 14.5 ka, when a thick package of fine-grained laminated sediments was deposited along the western Svalbard and Barents Sea continental slope (e.g. Jessen *et al*. 2010 and references therein). The southern Barents Sea is a likely source (Lucchi *et al*. 2013). Contemporaneous glacial re-advances have been suggested for Isfjorden and Kongsfjorden (Svendsen *et al*. 1996; Landvik *et al*. 2005).

While the main deglaciation of the MIS 2/1 transition into earliest Holocene lasted *c*. 6 ka (16.1–10.2 ka), the MIS 4/3 transition lasted longer according to the IRD record (Fig. 9). The deglaciation was apparently much slower and continued into early MIS 3 with pulsed deposition of local coarse-grained IRD for at least 10 ka (56–46 ka). Laminated sediments were also deposited during the MIS 4/3 transition (Vogt *et al*. 2001; Rasmussen & Thomsen 2013; Jessen & Rasmussen 2015), but were not as prominent as the layers dated to *c*. 14.5 ka. The slower deglaciation was probably a response to lower insolation and consistent with the less intense eustatic sea level rise of the MIS 4/3 transition (e.g. Martinson *et al*. 1987; Lambeck & Chappell 2001; Peltier & Fairbanks 2006).

Intervals of reduced ice-sheet size 46–30 ka and 10.2–0 ka. – The total IRD concentration in JM04-025PC was higher during the mid-late MIS 3 at 46–30 ka than during the Holocene (10.2–0 ka) (Fig. 9A). The cause is mainly a much higher abundance of allochthonous, fine-grained IRD in MIS 3, possibly due to higher inflow of sea ice from the Arctic Ocean, and a colder sea surface consistent with reduced ocean circulation and reduced inflow of Atlantic surface water (e.g. Ganopolski & Rahmstorf 2001; Hald *et al*., 2001; Rasmussen *et al*. 2003; van Meerbeck *et al*. 2009; Ezat *et al*. 2014) (Figs 6B, 9C).

Dates from molluscs from Novaya Zemlja indicate an ice-sheet extent similar to the present at *c*. 35 ka and probably even earlier (Mangerud *et al*. 2008). Local coarse-grained IRD was almost absent in core JM04-025PC during late MIS 3 (40–30 ka) indicating a rather passive ice margin and reduced ice-stream activity (Figs 9E, 10E). However, recent results from the upper slope of the northwestern Svalbard margin indicate a dynamic ice sheet with IRD deposition and deposition of laminated sediments from local meltwater plumes during MIS 3 and 4 (Rasmussen & Thomsen 2013). Also, studies of the activity of the Fennoscandian Ice Sheet (Olsen *et al*. 2002, 2013; Rørvik *et al*. 2010; Mangerud *et al*. 2011) and the British Ice Sheet (Scourse *et al*. 2009) indicate generally more active ice sheets than hitherto acknowledged. Between 39 and 36 ka, core JM03-374PC from the upper slope (1130 m water depth) displays significantly higher flux of IRD, lower percentages of quartz and higher grain-size ratio than at the site of core JM04-025PC indicating more iceberg rafting from local sources on the upper slope than further offshore (Fig. 11A–C). Between 34 and 31 ka the same differences in IRD flux and quartz percentages are seen (Fig. 11A,B). Thus, the reduction in local coarse-grained IRD in JM04-025PC at 40–30 ka could reflect that only a smaller proportion of local icebergs reached the outer slope (Fig. 10D). For example, local icebergs could have been relatively small and melting rapidly in Atlantic water over the upper part of the slope. Millennial-scale variability is still discernible in the IRD records as well as in the $\delta^{18}O$ records and in the magnetic susceptibility values (Figs 2B,C, 3B, 10B–E, 11A–C) (see also discussion below).

In core JM04-025PC in the Middle Holocene, an IRD pulse at *c*. 7.5 ka with more than 50% local, coarse-grained IRD is seen (Figs 4E,F, 9A,D, 10A,D). This event coincides with a rise in flux of mainly angular iceberg-rafted IRD in Isfjorden (Forwick & Vorren 2009). The icebergs apparently travelled far out over the slope. The event is not seen in core JM03-373PC further south (Fig. 4A,B), probably reflecting that the event was restricted to western Svalbard fjords and shelf, and that the prevailing surface current direction was south-to-north as today (e.g. Ślubowska *et al*. 2005; Rasmussen *et al*. 2007; Ślubowska-Woldengen *et al*. 2007; Skirbekk *et al*. 2010). The glaciers continued to grow during the Late Holocene with a culmination during the Little Ice Age (*c*. AD 1600–1850), when some glaciers were even larger than during the Younger Dryas (Svendsen & Mangerud 1997). The increase in IRD concentration is clearest in the fine-grained IRD composed of 50–60% quartz and 25–35% siltstones (Figs 4A,E, 7B,C, 9C,E, 10C,E). Coarse-grained IRD is almost absent (Figs 9B,D, 10B,D). Increasing IRD concentrations >150 μm have previously been interpreted as a sign of glacier growth, the neo-glaciation (Ślubowska *et al*. 2005; Ślubowska-Woldengen *et al*. 2007; Werner *et al*. 2011). However, based on the small grain-size, we suggest that a large proportion of the IRD in the Holocene sediments more likely is sea-ice rafted, and rather reflect the general cooling of the climate leading to the glacier growth.

Millennial-scale rhythm in IRD patterns

Interstadials and stadials. – The composition and grain-size ratio of the IRD show distinct millennial-scale variability (Figs 4B,D,F, 9B–E, 10B–E, 11). Periods of ice advance and peak glaciations (>74–63 ka and 30–16.1 ka) are dominated by allochthonous IRD. The few short-lived pulses of local IRD occur during interstadial warm inceptions GIS19 at *c*. 69 ka, GIS18 at 64 ka, GIS2 at 24–22 ka and at 18 ka. The latter event probably indicates a warming, which has also been recorded in the NGRIP ice core (Figs 9D, 10D).

During glacial retreat phases (56–46 and 16.1–10.2 ka) allochthonous IRD is rare (Fig. 9 B,C). Here we observe a distinct millennial-scale variation in the grain size of local IRD, most likely reflecting a change in the abundance of iceberg versus sea-ice rafted IRD. When the ice sheet was restricted to the Svalbard Archipelago (*c*. 46–30 and 10.2–0 ka), we observe a rhythmic shift between allochthonous, fine-grained IRD and local IRD (Fig. 10C–E). This millennial-scale pattern can to a large extent be caused by ocean temperature changes as also indicated by the distribution of IRD on orbital timescale (see above). In general, the cold stadial phases are nearly devoid of local, coarse-grained IRD.

According to the correlation to the Greenland ice core $\delta^{18}O$ (Fig. 6A,B), the local IRD peaks occur either during the early phase of the Greenland interstadials (GIS1; the Bølling–Allerød interstadials, GIS2, GIS4, GIS5, GIS10, GIS11, GIS14, GIS16 and GIS17) and/or well within the Greenland interstadials (GIS5, GIS9, GIS12, GIS13, GIS14, GIS15, GIS18, GIS19) (Fig. 10D). During all Greenland interstadials (except GIS6) local, coarse-grained IRD increase relative to local, fine-grained IRD (Fig. 10D,E) showing a coarsening of local IRD during warm intervals. Grain sizes of the IRD should be temperature independent and the coarsening probably signifies an increase in local iceberg calving and ice-sheet activity. The increased proportion and coarsening of local IRD during interstadials in combination with evidence of warm surface water flow over the upper slope (Rasmussen & Thomsen 2013), suggest increased calving and melting, when climate warmed. In general, the Svalbard-Barents Sea Ice Sheet was more dynamic under warmer climatic conditions (e.g. Elverhøi *et al*. 1995), which is supported by our data (Figs 9, 10, 11).

North Atlantic Heinrich Events. – During some Heinrich events (H5.2, H5, H4, H2 and H1), the presence of local coarse-grained IRD points to higher local calving activity than during the non-Heinrich stadials (Fig. 10D). However, the IRD concentration and flux is relatively low (with one exception of a short-lived spike during H4) and the actual calving rate of local icebergs was probably small (Figs 10A, 11A). Eventual calving events would have occurred in cold water (e.g. Bond *et al*. 1992, 1993; Dokken & Hald 1996) with low melting potential, and thus the IRD record might underestimate the calving and/or sediment load of icebergs. Calving of sediment-loaded icebergs into cold water would result in IRD from the Svalbard-Barents Sea Ice Sheet being deposited further away from Svalbard, which to our knowledge has only been reported for the above mentioned 24 ka IRD event (Bauch *et al*. 2001), and briefly during the last deglaciation at *c*. 14.5 ka (Bischof 1994). The high percentage of local, fine-grained IRD in some Heinrich events (H7, H5.2, H5, H4, H3 and H1) indicates extensive local sea-ice production in the Barents Sea and Svalbard western margin (Fig. 10E).

The distribution patterns of IRD in relation to climate at the western Svalbard margin is in contrast to most results from the Nordic Seas and North Atlantic. At the British margin, maxima in IRD occur at the end of stadials at the rapid warmings to interstadial climate (Scourse *et al*. 2009). A record from the central North Atlantic also showed maximum IRD deposition during warmings to the interstadials (Rasmussen *et al*. 2016), while in the western Irminger Sea it seems random if the IRD maxima (>150 μm) occur during stadial or interstadial climate (Elliott *et al*. 2001). Otherwise, the majority of IRD records from the

North Atlantic and southern Norwegian Sea show intensified ice rafting during the cold stadials (e.g. Heinrich 1988; Bond *et al*. 1992, 1993, 1999; Fronval *et al*. 1995; Bond & Lotti 1995; Rasmussen *et al*. 1996; Lackschewitz *et al*. 1998; van Kreveld *et al*. 2000; Moros *et al*. 2004). Most of these studies are based on cores more distal to iceberg sources than our cores from the western Svalbard slope, and from much lower latitudes. High IRD content recorded in cold climate in cores far away from ice sources and at low latitudes could be a result of the cold surface water allowing more icebergs to travel long distances and reach far (e.g. Bond & Lotti 1995; Bischof 2000). The melting of one iceberg can result in slower melting of the next. The extreme example is the Heinrich events, when IRD from Canada made it all the way to the southern Iberian margin (d'Errico & Sánchez Goñi 2003). A well-dated high-resolution core record from the margin off northern Portugal shows increased meltwater supply and cold surface temperatures a few centuries before the deposition of IRD (Naughton *et al*. 2009). Cooling of the surface waters was apparently necessary for icebergs to survive the travel across the North Atlantic. Similarly, the release of meltwater and icebergs from Svalbard, the British Ice sheet (Scourse *et al*. 2009) and possibly other ice sheets (Lekens *et al*. 2006) may have assisted in the long-distance transportation of IRD from Scandinavia, Iceland and Greenland to the North Atlantic during stadials by lowering of the surface water temperature in the Nordic seas and northeastern North Atlantic.

Influence of ocean temperature and travel routes for IRD provenance

The regional ocean surface temperature appears to play a significant part in the composition and provenance of the IRD west of Svalbard. In warmer surface water, the IRD melts out nearer its source, which will favour local IRD over allochthonous IRD. In colder surface water, icebergs and sea ice can transport IRD over long distances favouring the deposition of allochthonous IRD (see discussion above). The melting potential increases by an order or two of magnitude, when the surface water temperature rises from below 0 °C to +1–2 °C (Russel-Head 1980). Even a slight warming of regional surface water temperature can significantly increase the concentration of local IRD, and simultaneously restrict the deposition of allochthonous IRD since the higher melting rate reduces the distance ice can travel. Between 56 and 45 ka allochthonous IRD was absent in core JM04-025PC (Fig. 10B,C). The sea surface temperature in the North Atlantic during early MIS 3 was according to Kandiano *et al*. (2004), only 2 °C lower than today and probably too high for allochthonous IRD to reach Svalbard. Subsurface warming may trigger instability of outlet glaciers and ice shelves as recently suggested by Marcott *et al*. (2011), and as also observed in modern studies (e.g. Holland *et al*. 2008; Jeong *et al*. 2016). The peak in mainly local IRD and meltwater release during the warming phase would lead to surface water cooling (Rasmussen & Thomsen 2013) and subsequent gradual decrease in IRD concentration together with an increase in relative abundance of IRD from more distant sources due to reduced ice melt. The IRD patterns on the western Svalbard slope we present here during MIS 3 support this scenario. It is most clearly seen between H5 and H4. The Greenland interstadials GIS12–9 show a peak in local, coarse-grained IRD during peak interstadial warmth followed by a lowering of the IRD concentration and a peak in the relative abundance of allochthonous and fine grained IRD during the gradual cooling phase of the interstadials (Figs 9C,D, 10C,D).

Sea surface temperature and stadial-interstadial patterns in deposition of IRD

Even though the higher proportion of local, coarse-grained IRD points to more iceberg rafted

IRD during warm interstadial climate, it is uncertain if the increase is a sign of increased local calving activity or of warming of the ocean. A change in the thermal regime from cold-based to warm-based ice sheet should increase the calving rate and sediment load of icebergs by an order of magnitude (Elverhøi *et al*. 1995). However, the changing ocean temperature alone is also likely to affect IRD release, provenance and deposition, since a cold ocean surface can restrict the release of sediment-loaded icebergs to the open ocean (Andrews 2000). For example, during the cold stadials/Heinrich events and peak glaciations the fjords and shelf of Svalbard may have been covered with perennial sea ice, which potentially could have blocked the pathway for local icebergs and/or restricted the calving of icebergs (cf. Andrews 2000; Ó Cofaigh & Dowdeswell 2001; Hald & Korsun 2008; Forwick & Vorren 2009; Jongma *et al*. 2013). Before the icebergs are released, most of the sediment could have dropped out and icebergs would be 'clean' (Andrews 2000). Similarly, in a floating ice shelf, bottom melting can lead to a melt-out of most of the sediments prior to iceberg calving (e.g. Dowdeswell & Murray 1990; Domack *et al*. 1998). Together with the effect of slow ice melt in cold water, these mechanisms could significantly reduce the deposition of local IRD on the slope during cold, stadial climate independent of the iceberg calving rate. During the Greenland interstadial phases with Atlantic water at the surface (e.g. Rasmussen & Thomsen 2013), ice shelves would have retreated (cf. Sutter *et al.* 2016), fjords would be seasonally ice-free and icebergs could be released into the open ocean every year. The ice would thus melt close to its source with increased deposition of local IRD on the slope as a result.

The combination of high proportion, low concentration, and small grain-size of the allochthonous IRD during stadial climate (Fig 10A–C) mainly signifies that the sea surface temperature was cold enough for long-transportation of icebergs and sea ice. The high relative amount of allochthonous IRD during stadial phases is thus probably not directly proportional to the calving rate in distant places.

The overall IRD pattern on the west Svalbard slope with more local iceberg-IRD during Greenland interstadials and more allochthonous IRD during cold phases is probably a result of increased local glacial instability during warm interstadial climate. It is also very likely a result of regional changes in sea surface temperature affecting the transport and deposition of ice rafted sediment.

Conclusions

The grain-size and mineral composition of ice rafted detritus (IRD) on the west Svalbard slope was studied in three marine core records spanning 1130–1880 m water depth, covering together the last 74 ka (Marine isotope stages (MIS) 4–1). The results show that IRD shifted consistently on orbital- and millennial scales from allochthonous sources with dominance of fine and/or coarse quartz to predominantly IRD from local Svalbard-Barents Sea sources dominated by coarse Jurassic shales and siltstones.

During the glacial maxima of MIS 4 (74–56 ka) and MIS 2 (30–16.1 ka) including Heinrich events H6 and H1, respectively, the IRD on the western Svalbard margin was dominated by coarse, allochthonous IRD consisting of up to > 90% quartz and with almost no contributions from local sources. The Svalbard-Barents Sea Ice Sheet appeared to be stable with low ablation and we suggest that the modest ice loss during these cold glacial maxima facilitated the growth and stability of the ice sheet. At *c*. 24 ka increased ice stream activity caused a thinning of the Svalbard-Barents Sea Ice Sheet and a following intense calving of icebergs lead to rapid deglaciation of the outer shelf.

Calving of icebergs from the Svalbard-Barents Sea Ice Sheet and a high degree of instability of the ice sheet mainly occurred in relatively warm climate, for example during deglaciations and warm interstadials. During intervals of rapid deglaciation and ice retreat at the MIS 4/3 (56–46 ka) and MIS 2/1 (16.1–10.2 ka) transitions, ice rafting peaked over the western Svalbard slope and was dominated by deposition of local, coarse IRD, except for short time intervals of deposition of fine, laminated sediments. After these transitions, calving activity was low at 46–30 ka (mid-late MIS 3) and 10.2–0 ka (Holocene) and the IRD mostly consisted of fine-grained quartz deposited from sea ice interrupted by short events of deposition of coarse-grained, local IRD. In general, in MIS 4, MIS 3 and MIS 2 a clear millennial-scale pattern in ice rafting was observed with allochthonous quartz being deposited during cold Greenland stadials and Heinrich events and local shales/siltstones being deposited during the warm Greenland interstadials. The results show that the changes in ocean temperature probably enlarged these shifts in source of the IRD along with the stadial/interstadial climate cycles by prolonging the travel distance for ice and sediments during cold periods (allochthonous IRD) and shortening the distance in warm periods (local IRD).

Acknowledgements. – The investigation was supported in 2009–2012 by the University of Tromsø through the Research School in Arctic Marine Geology and Geophysics (AMGG) and the Mohn Foundation (project ‘Paleo-CIRCUS’). The project also received support from 2013 by the Research Council of Norway (Centre of Excellence funding scheme, grant no. 223259). The crew of *RV Jan Mayen* and engineer Steinar Iversen (UiT) are warmly thanked for their help in core retrieval, and Anders Solheim (NGI) for choosing the core sites of highest possible time resolution. Antoon Kuipers, Helga (Kikki) Flesche Kleiven and Jan

Sverre Laberg provided helpful comments on earlier versions of the manuscript. We thank the two reviewers Jens Bischof and James D. Scourse and the editor Jan A. Piotrowski for critical comments that significantly improved the manuscript.

References

Alexanderson, H., Landvik, J. Y., Molodkov, A. & Murray, A. S. 2011: A multi-method approach to dating middle and late Quaternary high relative sea-level events on NW Svalbard – a case study. *Quaternary Geochronology 6*, 326–340.

Alley, R. B. & MacAyeal, D. R. 1994: Ice-rafted debris associated with binge/purge oscillations of the Laurentide Ice Sheet. *Paleoceanography 9*, 503–511.

Andersen, E. S., Dokken, T. M., Elverhøi, A., Solheim, A. & Fossen, I. 1996: Late Quaternary sedimentation and glacial history of the Western Svalbard continental margin. *Marine Geology 133*, 123–156.

Andreassen, K., Laberg, J. S. & Vorren, T. O. 2008: Seafloor geomorphology of the SW Barents Sea and its glaci-dynamic implications. *Geomorphology 97*, 157–177.

Andrews, J. 2000: Icebergs and iceberg rafted detritus in the North Atlantic: facts and assumptions. *Oceanography 13*, 100–108.

Bauch, H. A., Erlendkeuser, H., Spielhagen, R. F., Struck, U., Matthiessen, J., Thiede, J. & Heinemeier J. 2001: A multiproxy reconstruction of the evolution of deep and surface waters in the subarctic Nordic seas over the last 30,000 yr. *Quaternary Science Reviews 20*, 659–678.

Benneth, M. 2003: Ice streams as the arteries of an ice sheet: their mechanics, stability and significance. *Earth-Science Reviews 61*, 309–339.

Bischof, J. 1994: The decay of the Barents Ice Sheet as documented in Nordic seas ice-rafted debris. *Marine Geology 117*, 35–55.

Bischof, J. F. 2000: *Ice Drift, Ocean Circulation and Climate Change*. 215 pp. Springer-Praxis, Cornwall.

Bischof, J. F. & Darby, D. A. 1997. Mid- to late Pleistocene Ice Drift in the western Arctic Ocean: Evidence for a different circulation in the past. *Science 277*, 74–77.

Bjarnadóttir, L. R., Rüther, D. C., Winsborrow, M. C. M. & Andreassen, K. 2012: Grounding-line dynamics during the last deglaciation of Kveithola, W Barents Sea, as revealed by seabed geomorphology and shallow seismic stratigraphy. *Boreas 42*, 84–107.

Bond, G. & Lotti, R. 1995: Iceberg discharge into the North Atlantic on millennial timescales during the last glaciations. *Science 267*, 1005–1010.

Bond, G., Heinrich, H., Broecker, W., Labeyrie, L., McManus, J., Andrews, J., Huon, S., Jantschik, R., Clasen, S., Simet, C., Tedesco, K., Klas, M., Bonati, G. & Ivy, S. 1992: Evidence for massive discharges of icebergs into the North Atlantic Ocean during the last glacial period. *Nature 360*, 245–249.

Bond, G., Broecker, W., Johnsen, S., McManus, J., Labeyrie, L., Jouzel, J. & Bonani, G. 1993: Correlations between climate records from North Atlantic and Greenland ice. *Nature 365*, 343–347.

Bond, G. C., Showers, W., Cheseby, M., Lotti, R., Almasi, P., deMenocal, P., Priore, P., Cullen, H., Hajdas, I. & Bonani, G. 1997: A pervasive millennial-scale cycle in North Atlantic Holocene and Glacial climates. *Science 278*, 1257–1266.

Bond, G. C., Showers, W., Elliot, M., Evans, M., Lotti, R., Hajdas, I., Bonani, G. & Johnsen, S. 1999: The North Atlantic's 1–2 kyr climate rhythm: Relation to Heinrich Events, Dansgaard/Oeschger cycles and the Little Ice Age. *In* Clark, P. U., Webb, R. S. & Keigwin, L. D. (eds.): *Mechanisms of Global Climate Change at Millennial Time Scales,* 35–58. *AGU Geophysical Monograph 112*.

Broecker, W., Bond, G. & Klas, M. 1990: A salt oscillator in the glacial Atlantic? 1. The concept. *Paleoceanography 5*, 469–477.

Broecker, W., Bond, G., Klas, M., Clark, E. & McManus, J. 1992: Origin of the northern Atlantic's Heinrich events. *Climate Dynamics 6*, 265–273.

Cadman, V. 1996: *Glacimarine sedimentation and environments during the late Weichselian and Holocene in the Bellsund Through and van Keulenfjorden, Svalbard*. Ph. D. thesis, University of Cambridge, 250 pp.

Chappell, J. 2002: Sea level changes forced ice breakouts in the Last Glacial cycle: new results from coral terraces. *Quaternary Science Reviews 21*, 1229–1240.

Chauhan, T., Rasmussen, T. L., Noormets, R., Jakobsson, M. & Hogan, K. A. 2014: Glacial history and paleoceanography of the southern Yermak Plateau since 132 ka BP. *Quaternary Science Reviews* 92, 155–169.

Dahlgren, K. I. & Vorren, T. O. 2003: Sedimentary environment and glacial history during the last 40 ka of the Vøring continental margin, mid-Norway. *Marine Geology 193*, 93–127.

Dansgaard, W., Johnsen, S. J., Clausen, H. B., Dahl-Jensen, D., Gundestrup, N. S., Hammer, C. U., Hvidberg, C. S., Steffensen, J., Sveinbjörnsdottir, A. E., Jouzel, J. & Bond, G. 1993: Evidence for general instability of past climate from a 250-kyr ice-core record. *Nature 364*, 218–220.

d'Errico, F. & Sánchez-Goñi, M. F. 2003: Neanderthal extinction and the millennial scale climatic variability of OIS 3. *Quaternary Science Reviews 22*, 769–788.

Dimakis, P., Elverhøi, A., Høeg, K., Solheim, A., Harbitz, C., Laberg, J. S., Vorren, T. O. & Marr, J. 2000: Submarine slope stability on high-latitude glaciated Svalbard–Barents Sea margin. *Marine Geology 162*, 303–316.

Dokken, T. & Hald, M. 1996: Rapid climatic shifts during isotope stages 2–4 in the Polar North Atlantic. *Geology 24*, 599–602.

Domack, E. W. & Harris, P. T. 1998: A new depositional model for ice shelves, based upon sediment cores from the Ross Sea and the MacRobertson shelf, Antarctica. *Annals of Glaciology 27*, 281–284.

Dowdeswell, J. A. & Dowdeswell, E. K. 1989: Debris in icebergs and rates of glacimarine sedimentation: observations from Spitsbergen and a simple model. *Journal of Geology 97*, 221–231.

Dowdeswell, J. A. & Murray, T. 1990: Modelling rates of sedimentation from icebergs. *In* Dowdeswell, J. A. & Scourse, J. D. (eds.): *Glacimarine Environments: Processes and Sediments*, 121–137. *Geological Society, London, Special Publication 53*.

Edwards, M. B. 1975. Gravel fraction on the Spitsbergen Bank, NW Barents shelf. *Norges Geologiske Undersøkelse Bulletin 316*, 205–217.

Eiken, O. & Hinz, K. 1993: Contourites in the Fram Strait. *In* Stow, D. A. & Faugères, J. -C. (eds.): *Contourites and Bottom Currents*, 15–32. *Sedimentary Geology 82*.

Eldevik, T., Nilsen, J. E. Ø., Iovino, D., Olsson, K. A., Sandø, A. B. & Drange, H. 2009: Observed sources and variability of Nordic seas overflow. *Nature Geoscience 2*, 406–410.

Elliott, M., Labeyrie, L. Dokken, T. & Manthé, S. 2001: Coherent patterns of ice-rafted debris deposits in the Nordic regions during the last glacial (10–60 ka). *Earth and Planetary Science Letters 194*, 151–163.

Elverhøi, A., Andersen, E. S., Dokken, T., Hebbeln, D., Spielhagen, R., Svendsen, J. I., Sørflaten, M., Rørnes, A., Hald, M. & Forsberg, C. F. 1995: The growth and decay of the Late Weichselian Ice Sheet in Western Svalbard and adjacent areas based on provenance studies of marine sediments. *Quaternary Research 44*, 303–316.

Elverhøi, A., Hooke, R. L. E. B. & Solheim, A. 1998: Late Cenozoic erosion and sediment yield from the Svalbard-Barents Sea region: implications for understanding erosion of glacierized basins. *Quaternary Science Reviews 17*, 209–241.

Ezat, M., Rasmussen, T. L. & Groeneveld, J. 2014: Persistent intermediate water warming during cold stadials in southern Nordic seas during the past 65 k.y. *Geology 42*, 663–666.

Forwick, M. & Vorren, T. O. 2009: Late Weichselian and Holocene sedimentary environments and ice rafting in Isfjorden, Spitsbergen. *Paleogeography, Paleoclimatology, Paleoecology 280*, 258–274.

Fronval, T., Jansen, E. Bloemendal, J. & Johnsen, S. 1995: Oceanic evidence for coherent fluctuations in Fennoscandian and Laurentide ice sheets on millennium timescales. *Nature 374*, 443–446.

Ganopolski, A. & Rahmstorf, S. 2001: Rapid changes of glacial climate simulated in a coupled climate model. *Nature 409*, 153–158.

Gildor, H. & Tziperman, E. 2001: A sea ice climate switch mechanism for the 100-kyr glacial cycles. *Journal of Geophysical Research 106*, 9117–9136.

Gjermundsen, E. F., Briner, J. P., Akcar, N., Salvigsen, O., Kubik, P., Gantert, N. & Hormes, A. 2013: Late Weichselian local ice dome configuration and chronology in Northwestern Svalbard: early thinning, late retreat. *Quaternary Science Reviews 72*, 112–127.

Goldschmidt, P. M. 1995: Accumulation rates of coarse-grained terrigenous sediment in the Norwegian-Greenland Sea: signals of continental glaciation. *Marine. Geology 128*, 137–151.

Grundvåg, S. A. & Olaussen, S. 2017: Sedimentology of the Lower Cretaceous at Kikutodden and Keilhaufjellet, southern Spitsbergen: implications for an onshore-offshore link. *Polar Research 36*, doi:10.1080/17518369.2017.1302124.

Hald, M. & Korsun, S. 2008: The 8200 cal. yr BP event reflected in the Arctic fjord, Van Mijenfjorden, Svalbard. *The Holocene 18*, 981–990.

Hald, M., Dokken, T. M. & Mikaelsen, G. 2001: Abrupt climatic change during the last interglacial–glacial cycle in the polar North Atlantic. *Marine Geology 176*, 121–137.

Hebbeln, H. 2000: Flux of ice-rafted detritus from sea ice in the Fram Strait. *Deep Sea Research II 47*, 1773–1790.

Hebbeln, D. & Wefer, G. 1997: Late Quaternary paleoceanography in the Fram Strait. *Paleoceanography 12*, 65–78.

Hebbeln, D., Dokken, T., Andersen, E. S., Hald, M. & Elverhøi, A. 1994: Moisture supply for northern ice sheet growth during the last Glacial Maximum. *Nature 370*, 357–360.

Heinrich, H. 1988: Origin and consequences of cyclic ice rafting in the Northeast Atlantic Ocean during the past 130,000 years. *Quaternary Research 29*, 142–152.

Hjelstuen, B. O., Elverhøi, A. & Falaide, J. I. 1996: Cenozoic erosion and sediment yield in the drainage area of the Storfjorden Fan. *Global and Planetary Change 12*, 95–117.

Hogan, K. A., Dowdeswell, J. A., Noormets, R., Evans, J., Ó Cofaigh, C. & Jakobsson, M. 2010: Submarine landforms and ice-sheet flow in the Kvitøya Trough, northwestern Barents Sea. *Quaternary Science Reviews 49*, 3545–3562.

Holland, D. M., Thomas, R. H., de Young, B., Ribergaard, M. H. & Lyberth, B. 2008: Acceleration of Jacobshavn Isbræ triggered by warm subsurface ocean waters. *Nature Geoscience 1*, 659–664.

Hopkins, T. S. 1991: The GIN Sea – A synthesis of its physical oceanography and literature review 1972–1985. *Earth-Science Reviews 30*, 175–318.

Hormes, A., Gjermundsen, E. F. & Rasmussen, T. L. 2013. From mountain top to the deep sea – deglaciation in 4D of the northwestern Barents Sea ice sheet. *Quaternary Science Reviews 75*, 78–99.

Howe, J. A., Shimmels, T. M., Harland R. & Eyles, N. 2008: Late Quaternary contourites and glaciomarine sedimentation in the Fram Strait. *Sedimentology 55*, 179–200.

Hughes, T. 1996: Can ice sheets trigger abrupt climatic change? *Arctic and Alpine Research 28*, 448–465.

Hughes, T. 2002: Calving Bays. *Quaternary Science Reviews 21*, 267–282.

Hulbe, C. L. 1997: An ice shelf mechanism for Heinrich layer production. *Paleoceanography 12*, 711–717.

Hulbe, C. L., MacAyeal, D. R., Denton, G. H., Kleman, J. & Lowell, T. V. 2004: Catastrophic ice shelf breakup as the source of Heinrich event icebergs. *Paleoceanography 19*, PA1004, doi:10.1029/2003PA000890.

Jenkins, A. 1991: A one-dimensional model of ice shelf-ocean interaction. *Journal of Geophysical Research 96(C11)*, 20,671–20,677.

Jeong, S., Howat, I. M. & Bassis, J. N. 2016: Accelerated ice shelf rifting and retreat at Pine Island Glacier, West Antarctica. *Geophysical Research Letters 43*, 11,720–11,725.

Jessen, S. P. 2005: *Dangaard/Oeschger cycler på Svalbardmarginen*. Cand. Scient. thesis, University of Copenhagen, 73 pp.

Jessen, S. P. & Rasmussen, T. L. 2015: Sortable silt cycles in Svalbard slope sSediments 74–0 ka. *Journal of Quaternary Science 30*, 743–753.

Jessen, S. P., Rasmussen, T. L., Nielsen, T. & Solheim, A. 2010: A new Late Weichselian and Holocene marine chronology for the western Svalbard slope 30,000 – 0 cal years BP. *Quaternary Science Reviews 29*, 1301–1312.

Jongma, J. I., Renssen, H. & Roche, D. M. 2013: Simulating Heinrich event 1 with interactive icebergs. *Climate Dynamics 40*, 1373–1385.

Kandiano, E. S., Bauch H. A. & Müller, A. 2004: Sea surface temperature variability in the North Atlantic during the last two glacial-interglacial cycles: comparison of faunal, oxygen isotopic, and Mg/Ca-derived records. *Paleogeography, Paleoclimatology, Paleoecology 204,* 145–164.

Kelly, S. R. A. 1988: Jurassic through Cretaceous Stratigraphy of the Barents Shelf. *In* Harland, W. B. & Dowdeswell, E. K. (eds.): *Geological Evolution of the Barents Shelf Region*, 109–130. Graham and Trotman, London.

Knies, J., Vogt, C. & Stein, R. 1999: Late Quaternary growth and decay of the Svalbard/Barents Sea ice sheet and paleoceanographic evolution in the adjacent Arctic Ocean. *Geo-Marine Letters 18*, 195–202.

Kolla, V., Biscaye, P. E. & Hanley, A. F. 1979: Distribution of Quartz in late Quaternary Sediments in Relation to Climate. *Quaternary Research 11*, 261–277.

van Kreveld, S., Sarnthein, M., Erlenkeuser, H., Grootes, P., Jung, S., Nadeau, M. J., Pflaumann, U. & Voelker, A. 2000: Potential links between surging ice sheets, circulation changes, and the Dansgaard-Oeschger cycles in the Irminger Sea, 60–18 kyr. *Paleoceanography 15*, 425–442.

Laberg, J. S. & Vorren, T. O. 1995: Late Weichselian submarine debris flow deposits on the Bear Island Trough Mouth Fan. *Marine Geology 127*, 45–72.

Lackschewitz, K. S., Baumann, K.-H., Gehrke, B., Wallrabe-Adams, H. –J., Thiede, J., Bonani, G., Endler, R., Erlenkeuser, H. & Heinemeier, J. 1998: North Atlantic ice sheet fluctuations 10,000–70,000 yr ago as inferred from deposits on the Reykjanes Ridge, southeast of Greenland. *Quaternary Research 49*, 171–182.

Lambeck, K. & Chappell, J. 2001: Sea level change through the last glacial cycle *Science 292*, 679–685.

Lambeck, K. 2004: Sea-level change through the last glacial cycle: geophysical, glaciological and palaeogeographic consequences. *Comptes Rendus Geosciences 336*, 677–689.

Landvik, J. Y., Ingólfsson, Ó., Mienert, J., Lehman, S. J., Solheim, A., Elverhøi, A. & Ottesen, D. 2005: Rethinking Late Weichselian ice-sheet dynamics in coastal NW Svalbard. *Boreas 34*, 7–24.

Landvik, J. Y., Brook, E. J., Gualtieri, L., Linge, H., Raisbeck, G., Salvigsen, O. & Yiou, F. 2013: ^{10}Be exposure age constraints on the Late Weichselian ice sheet geometry and dynamics in inter ice-stream areas, western Svalbard. *Boreas 42*, 43–56.

Landvik, J. Y., Alexanderson, H., Henriksen, M. & Ingólfsson, Ó. 2014: Landscape imprints of changing glacial regimes during ice-sheet build-up and decay: a conceptual model from Svalbard. *Quaternary Science Reviews 92*, 258–268.

Leinen, M., Cwienk, D., Heath, G. R., Biscaye, P. E., Kolla, V., Thiede, J. & Dauphin, J. P. 1986: Distribution of biogenic silica and quartz in recent deep-sea sediments. *Geology 14*, 199–203.

Lekens, W. A. H., Sejrup, H. P., Haflidason, H., Knies, J. & Richter, T. 2006: Meltwater and ice rafting in the southern Norwegian Sea between 20 and 40 calendar kyr B.P.: Implications for Fennoscandian Heinrich events. *Paleoceanography 21*, doi:10.1029/2005PA001228.

Lekens, W. A. H., Sejrup, H. P., Haflidason, H., Petersen, G. Ø., Hjelstuen, B. & Knorr, G. 2005: Laminated sediments preceding Heinrich Event 1 in Northern North Sea and Southern Norwegian Sea: Origin, processes and regional linkage. *Marine Geology 216*, 27–50.

Lucchi, R. G., Camerlenghi, A., Rebesco, M., Colmenero-Hidalgo, E., Siero, F. J., Sagnotti, L., Urgeles, R., Melis, R., Morigi, C., Bárcena, M.-A., Giorgetti, G., Villa, G., Persico, D., Flores, J.-A., Rigual-Hernandez, A. S., Pedrosa, M. T., Macri, P. & Caburlotto, A. 2013: Postglacial sedimentary processes on the Storfjorden and Kveithola trough mouth fans: Significance of extreme glacimarine sedimentation. *Global and Planetary Change 111*, 309–326.

Lundschien, B. A., Høy, T. & Mørk, A. 2014: Triassic hydrocarbon potential in the Northern Barents Sea; integrating Svalbard and stratigraphic core data. *Norwegian Petroleum Directorate Bulletin 11*, 3–20.

Maher, H. D. jr., Hays, T., Shuster, R. & Mutrux, J. 2004: Petrography of Lower Cretaceous sandstones on Spitsbergen. *Polar Research 23*, 147–165.

Mangerud, J., Dokken. T., Hebbeln, D., Heggen, B., Ingólfsson, Ó., Landvik, J. Y., Mejdahl, V., Svendsen, J. I. & Vorren, T. O. 1998: Fluctuations of the Svalbard-Barents Sea Ice Sheet during the last 150 000 years. *Quaternary Science Reviews 17*, 11–42.

Mangerud, J., Kaufman, D. & Hansen, J. 2008: Ice-free conditions in Novaya Zemlya 35 000–30 000 cal years B.P., as indicated by radiocarbon ages and amino acid racemization evidence from marine mollusks. *Polar Research 27*, 187–208.

Mangerud, J., Gyllencreutz, R., Lohne, Ø. & Svendsen, J. I. 2011: Glacial history of Norway. *In* Ehlers, J., Gibbard, P. & Hughes, P. (eds.): *Quaternary Glaciations – Extent and Chronology*, 279–298. Elsevier, Amsterdam.

Marcott, S. A., Clark, P. U., Padman, L., Klinkhammer, G. P., Springer, S. R., Liu, Z., Otto-Bliesner, B. L., Carlson, A. E., Ungerer, A., Padman, J., He, F., Cheng J. & Schmittner, A. 2011: Ice-shelf collapse from subsurface warming as trigger for Heinrich events. *PNAS 108*, 13,415–13,419.

Martinson, D. G., Pisias, N., Nicklas, G., Hays, J. D., Imbrie, J. D., Moore, T. C. & Shackleton, N. J. 1987: Age dating and the orbital theory of the ice ages: development of a high-resolution 0 to 300,000-year chronostratigraphy. *Quaternary Research 27*, 1–29.

van Meerbeck, C. J., Renssen, H. & Roche, D. M. 2009: How did Marine Isotope Stage 3 and Last Glacial Maximum climates differ? – Perspectives from equilibrium simulations. *Climate of the Past 5*, 33–51.

Moros, M., Emeis, K., Risebrobakken, B., Snowball, I., Kuipers, A., McManus, J. & Jansen, E. 2004: Sea surface temperature and ice rafting in the Holocene North Atlantic: climate influences on northern Europe and Greenland. *Quaternary Science Reviews 23*, 2113–2126.

Naugthon, F., Sánchez-Goñi, M. F., Kageyama, M., Bard, E., Duprat, J., Cortijo, E., Desprat, S., Malaizé, B., Joly, C., Rostek, F. & Turon, J. -L. 2009: Wet to dry climatic trend in north-western Iberian within Heinrich events. *Earth and Planetary Science Letters*

284, 329–342.

NGRIP Members 2004: High-resolution record of Northern Hemisphere climate extending into the last interglacial period. *Nature 431*, 147–151.

Nielsen, T. & Rasmussen, T. L. 2018: Reconstruction of ice sheet retreat after the Last Glacial Maximum in Storfjorden, southern Svalbard. *Marine Geology 402*, 228–242.

Ó Cofaigh, C. & Dowdeswell, J. A. 2001: Laminated sediments in glacimarine environments: diagnostic criteria for their interpretation. *Quaternary Science Reviews 20*, 1411–1436.

Olsen, L., Sveian, H., van der Borg, L., Bergstrøm, B. & Broekmans, M. 2002: Rapid and rhythmic ice sheet fluctuations in western Scandinavia 15–40 Kya – a review. *Polar Research 21*, 235–242.

Olsen, L., Sveian, H., Ottesen, D. & Rise, L. 2013: Quaternary glacial, interglacial and interstadial deposits of Norway and adjacent onshore and offshore areas. *In* Olsen, L., Fredin, O. & Olesen O. (eds.): *Quaternary Geology of Norway*, 79–144. *Geological Survey of Norway Special Publication 13*.

Ottesen, D., Dowdeswell, J. A. & Rise, L. 2005: Submarine landforms and the reconstruction of fast-flowing ice streams within a large Quaternary ice sheet: the 2500 km-long Norwegian-Svalbard margin (57º to 80ºN). *Geological Society of America Bulletin 117*, 1033–1050.

Ottesen, D., Dowdeswell, J. A., Landvik, J. Y. & Mienert, J. 2007: Dynamics of the Late Weichselian ice sheet on Svalbard inferred from high-resolution sea-floor morphology. *Boreas 36*, 286–306.

Patton, H., Andreassen, K., Bjarnadóttir, L. R., Dowdeswell, J. A., Winsborrow, M. C. M., Noormets, R., Polyak, L., Auriac, A. & Hubbard, A. 2015: Geophysical constraints on the dynamics and retreat of the Barents Sea ice sheet as a paleobenchmark for models of marine ice sheet deglaciation. *Reviews of Geophysics 53*, 1051–1098.

Peltier, W. R. & Fairbanks, R. G. 2006: Global glacial ice volume and Last Glacial Maximum duration from an extended Barbados sea level record. *Quaternary Science Reviews 25,* 3322–3337.

Pfirman, S., Wollenburg, J., Thiede, J. & Lange, M. A. 1989: Lithogenic sediments on Arctic pack ice: potential aeolian flux and contributions to deep sea sediments. *In* Sarnthein, M. & Leinen, M. (eds.): *Paleoclimatology and Paleometeorology: Modern and Past Patterns of Global Atmospheric Transport*, 463–493. Kluwer, Dordrecht.

Rasmussen, T. L. & Thomsen, E. 2013: Pink marine sediments reveal rapid ice melt and Arctic meltwater discharge during Dansgaard-Oeschger warmings. *Nature Communications 4*, doi: 10.1038/ncomms3849.

Rasmussen, T. L., Thomsen, E. & Moros, M. 2016: North Atlantic warming during Dansgaard-Oeschger events synchronous with Antarctic warming and out-of-phase with Greenland climate. *Scientific Reports 6*, doi:10.1038/srep20535.

Rasmussen, T. L., Thomsen, E. & Nielsen, T. 2014: Water mass exchange between the Nordic seas and the Arctic Ocean on millennial time scale during MIS 4–MIS 2. *Geochemistry, Geophysics, Geosystems 15*, 530–544.

Rasmussen, T. L., Thomsen, E., Ślubowska, M. A., Jessen, S. P., Solheim, A. & Koç, N. 2007: Paleoceanographic evolution of the SW Svalbard margin (76°N) since 20,000

^{14}C yr BP. *Quaternary Research 67*, 100–114.

Rasmussen, T. L., Thomsen, E., Troelstra, S. R., Kuipers, A. & Prins, M. A. 2003: Millennial-scale glacial variability versus Holocene stability: changes in planktic and benthic foraminifera faunas and ocean circulation in the North Atlantic during the last 60,000 years. *Marine Micropaleontology 47*, 143–176.

Rasmussen, T. L., Thomsen, E., van Weering, T. C. E. & Labeyrie, L. 1996: Rapid changes in surface and deep water conditions at the Faeroe Margin during the last 58,000 years. *Paleoceanography 11*, 757–771.

Rebesco, M., Laberg, J. S., Pedrosa, M. T., Camerlenghi, A., Lucchi, R. G., Zgur, F. & Wardell, N. 2014: Onset and growth of Trough-Mouth Fans on the North-Western Barents Sea margin – implications for the evolution of the Barents Sea/Svalbard Ice Sheet. *Quaternary Science Reviews 92*, 227–234.

Reimer, P. J., Edouard, B., Bayliss, A., Beck, J. W., Blackwell, P. G., Ramsey, C. B., Buck, C. E., Cheng, H., Edwards, R. L., Friedrich, M., Grootes, P. M., Guilderson, T. P., Haflidason, H., Hajdas, I., Hatté, C., Heaton, T. J., Hoffmann, D. L., Hogg, A. G., Hughen, K. A., Kaiser, K. F., Kromer, B., Manning, S. W., Nju, M., Reimer, R. W., Richards, D. A., Scott, E. M., Southon, J. R., Staff, R. A., Turney, C. S. M. & van der Plicht, J. 2013: INTCAL13 and Marine13 radiocarbon age calibration curves 0–50,000 years cal BP. *Radiocarbon 55*, 1869–1886.

Ruddiman, W. F. 1977: Late Quaternary deposition of ice-rafted sand in subpolar North Atlantic (lat 40 to 65 N). *Geology 88*, 1813–1827.

Russel-Head, D. D. 1980: Melting of free-drifting icebergs. *Annals of Glaciology 1*, 119–122.

Rüther, D. C., Bjarnadóttir, L. R., Junttila, J., Husum, K., Rasmussen, T. L., Lucchi, R. G. & Andreassen, K. 2012: Pattern and timing of the north-western Barents Sea Ice Sheet deglaciation and indications of episodic Holocene deposition. *Boreas 41*, 494–512.

Rørvik, K. -L., Laberg, J. S., Hald, M., Ravna, E. K. & Vorren, T. O. 2010: Behavior of the northwestern part of the Fennoscandian Ice Sheet during the Last Glacial Maximum – a response to external forcing. *Quaternary Science Reviews 29*, 2224–2237.

Scourse, J. D., Haapaniemi, A. I., Colmenero-Hidalgo, E., Peck, V. L., Hall, I. R., Austin, W. E. N., Knutz, P. C. & Zahn, R. 2009: Growth, dynamics and deglaciation of the last British-Irish ice sheet: the deep-sea ice-rafted detritus record. *Quaternary Science Reviews 28*, 3066–3084.

Shaffer, G., Olsen, S. M. & Bjerrum, C. J. 2004: Ocean subsurface warming as a mechanism for coupling Dansgaard-Oeschger climate cycles and ice-rafting events. *Geophysical Research Letters 31*, L24202, doi:10.1029/2004GL020968.

Siegert, M. J. & Dowdeswell, J. A. 2002: Late Weichselian iceberg, surface-melt and sediment production from the Eurasian Ice Sheet: results from numerical ice-sheet modelling. *Marine Geology 198*, 109–127.

Siegert, M. J. & Dowdeswell, J. A. 2004, Numerical reconstructions of the Eurasian Ice Sheet and climate during the Late Weichselian. *Quaternary Science Reviews 23*, 1273–1283.

Skirbekk, K., Klitgaard-Kristensen, D., Rasmussen, T. L., Koç, N. & Forwick, M. 2010; Holocene climate variations at the entrance to a warm Arctic fjord: Evidence from

Kongsfjorden Trough, Svalbard. *Geological Society, London, Special Publications 344*, 289–304.

Ślubowska, M. A., Koç, N., Rasmussen, T. L. & Klitgaard-Kristensen, D. 2005: Changes in the flow of Atlantic water into the Arctic Ocean since the last deglaciation: Evidence from the northern Svalbard continental margin, 80°N. *Paleoceanography 20*, PA4014, doi:10.1029/2005PA001141.

Ślubowska-Woldengen, M., Rasmussen, T. L., Koç, N., Klitgaard-Kristensen, D., Nilsen F. & Solheim, A. 2007: Advection of Atlantic Water to the western and northern Svalbard shelf since 17,500 cal yr BP. *Quaternary Science Reviews 26*, 463–478.

Snowball, I., Nilsson, A. &. Rasmussen, T. L. 2007: Late Quaternary geomagnetic excursions at high northern latitudes in marine sediments: reproducing results for the wrong reasons? *Eos Transactions AGU 88*, GP21A-0099.

Spielhagen, R. F. 1991: Die Eisdrift in der Framstraße während der letzten 200000 Jahre. *GEOMAR Report 4*, 1–137.

Stuiver, M. & Reimer, P. 1993: Extended ^{14}C database and revised Calib 3.0 age calibration program. *Radiocarbon 35*, 215–230.

Sutter, J., Gierz, P., Grosfeld, K., Thoma, M. & Lohmann, G. 2016: Ocean temperature thresholds for last interglacial West Antarctic Ice Sheet collapse. *Geophysical Research Letters 43*, 2675–2682.

Svendsen, J. I. & Mangerud J. 1997: Holocene glacial and climatic variations on Spitsbergen, Svalbard. *The Holocene 7*, 45–57.

Svendsen, J. I., Elverhøi, A. & Mangerud, J. 1996: The retreat of the Barents Ice Sheet on the western Svalbard margin. *Boreas 25*, 244–256.

Svendsen, J. I., Alexanderson, H., Astakhov, V., Demidov, J., Dowdeswell, J. A., Henriksen, M., Hjort, C., Houmark-Nielsen, M., Hubberten, H., Ingólfsson, Ó., Jakobsson, M., Kjær, K., Larsen, E., Lokrantz, H., Luunka, E. P., Lyså, A., Mangerud, J., Maslenikova, O., Matioushkov, A., Murray, A., Möller, P., Niessen, F., Saarnisto, M., Siegert, M., Stein, R. & Spielhagen, R. 2004. Ice sheet history of northern Eurasia. *Quaternary Science Reviews 22*, 1229–1271.

Sztybor, K. & Rasmussen, T. L. 2017: Diagenetic disturbances of marine sedimentary records from methane influenced environments in the Fram Strait as indications for variation in seep intensity during the last 35 000 years. *Boreas 46*, 212–228.

Vogt, C., Knies, J. Spielhagen, R. F. & Stein R. 2001: Detailed mineralogical evidence for two nearly identical glacial/deglacial cycles and Atlantic water advection to the Arctic Ocean during the last 90,000 years. *Global and Planetary Change 31*, 23–44.

Vorren, T. O., Lebesbye, E., Andreassen, K. & Larsen, K. -B. 1989: Glacigenic sediments on a passive continental margin as exemplified by the Barents Sea. *Marine Geology 85*, 251–272.

Vorren, T. O. & Laberg, J. S. 1997: Trough mouth fans – Paleoclimate and ice-sheet monitors. *Quaternary Science Reviews 16*, 865–881.

Wagner, T. & Henrich R. 1994: Organo- and lithofacies of glacial-interglacial deposits in the Norwegian-Greenland Sea: Responses to paleoceanographic and paleoclimatic changes. *Marine Geology 120*, 335–364.

Werner, K., Spielhagen, R. F., Bauch, D., Hass, H. C., Kandiano, E. S. & Zamelczyk, K. 2011: Atlantic Water advection to the eastern Fram Strait - multiproxy evidence for late Holocene variability. *Palaeogeography, Palaeoclimatology, Palaeoecology 308*, 264–276.

Winsborrow, M. C. M., Andreassen, K., Corner, G. D. & Laberg, J. S. 2010: Deglaciation of a marine-based ice sheet: Late Weichselian paleo-ice dynamics and retreat in the southern Barents Sea reconstructed from onshore and offshore glacial geomorphology. *Quaternary Science Reviews 29*, 424–442.

Young N. E., Lamp, J., Koffman, T., Briner, J. P., Schaefer, J., Gjermundsen, E., Linge, H., Zimmerman, S., Guilderson, T. P., Fabel, D. & Hormes, A. 2018: Deglaciation of coastal south-western Spitsbergen dated with *in situ* cosmogenic ^{10}BE and ^{14}C measurements. *Journal of Quarternary Science*, 1–14, doi: 10.1002/jqs.3058.

Zhang X., Prange, M., Merkel U. & Schulz, M. 2014: Instability of the Atlantic overturning circulation during Marine Isotope Stage 3. *Geophysical Research Letters 41*, 4285–4293.

Figure captions

Fig. 1. (A) Map of Nordic seas showing main surface (red) and bottom (blue) currents and locations of investigated cores (black circles). Location of core PS1243 discussed in the text (purple circle) (Bauch *et al*. 2001) is also marked. (B) Location of investigated cores (black circles) and core JM05-031GC used for correlation and age models (blue circle) (Rasmussen *et al*. 2014). Northward flow path of Atlantic Water is indicated (red arrow). Areas of Jurassic shales and siltstones at Spitsbergen Bank (blue-green) and Lower Cretaceous quartz-rich deposits (orange) are indicated (sketched after Edwards (1975), Maher *et al*. (2004) and Grundvåg & Olausson (2017)).

Fig. 2. Magnetic susceptibility records of (A) JM03-373PC, (B) JM04-025PC, (C) JM03-374PC correlated with (D) JM05-031GC from Rasmussen *et al*. (2014). AMS^{14}C dated levels

are marked with red diamonds. Magnetic susceptibility tie-points (tp) 1–9 from Jessen *et al*. (2010) are marked. Also, a diatom-rich layer, laminated meltwater deposits (light grey bars) and mass-transport deposits (dark grey bar) are shown (Jessen *et al*. 2010). The location of the Laschamps event (semi-dark grey bar) (Snowball *et al*. 2007) and North Atlantic Heinrich Event 1 and 6 (H1 and H6) (light blue bars) are indicated. An additional MS correlation point is shown (dotted line). Marine Isotope Stages (MIS) are shown in column to the left.

Fig. 3. Previously published oxygen Isotope records of (A) JM03-373PC (Rasmussen *et al*. 2007; Jessen *et al*. 2010), (B) JM04-025PC (Jessen & Rasmussen 2015), (C) JM03-374PC (Jessen & Rasmussen 2015) correlated with JM05-031GC from Rasmussen *et al*. (2014) (D,E). Records (A,B) and (E) are measured on planktic foraminiferal species *Neogloboquadrina pachyderma* s (NPS), while (C) and (D) are measured on benthic foraminiferal species. AMS^{14}C dated levels are marked with red diamonds. Additional ^{18}O correlation points are shown with dotted lines. Legend otherwise as in Fig. 2.

Fig. 4. Concentration of Ice Rafted Detritus (IRD) >500 µm and 150–500 µm in number per gram dry weight sediment and normalized grain-size ratio (see text for explanation) on cm scale for (A,B) JM03-373PC, IRD concentration >150 µm from Rasmussen *et al*. (2007), IRD concentration >500 µm from Jessen *et al*. (2010), (C,D) JM03-374PC (IRD concentrations from Jessen (2005)) and (E,F) JM04-025PC (IRD concentration >500 µm, 500–0 cm from Jessen *et al*. (2010)). Tie points (tp, including new tie point tp 6.1; see legend Fig. 2) and selected AMS ^{14}C dates are indicated.

Fig. 5. Age-depth plots of JM03-373PC, JM04-025PC and JM03-374PC with lithologic units

(Jessen *et al*. 2010) and Laschamps event (Snowball *et al*. 2007) indicated. See also legend to Fig. 2.

.

Fig. 6. Correlation between (A) $\delta^{18}O$ record of Greenland NGRIP ice core (data from NGRIP Members 2004) and (B) grain-size of sortable silt in core JM04-025PC with horizontal green bars marking location of laminated clay layers (data from Jessen & Rasmussen 2015). Marine isotope stages (MIS) are indicated (right column).

Fig. 7. IRD data of core JM04-025PC plotted versus age. A. Concentration of IRD in number per gram dry weight sediment. B,C. % quartz and % siltstones of total IRD. D. Normalized grain-size ratio, where 1 is average of the core and >1 is coarser than average and <1 is finer than average. Marine Isotope Stages (MIS) are marked in right column. Location of a mass-transport deposit at 24 ka is marked with grey bar.

Fig. 8. A. Scatter plot of % siltstones versus % quartz in JM04-025PC. B. Scatter plot of concentration of IRD 150–500 µm versus IRD >500 µm in JM04-025PC. For explanation see text in Section ‘Local versus allochthonous IRD’.

Fig. 9. A. Concentration of IRD >250 µm in number per gram dry weight sediment divided into four end-members: (B) allochthonous, coarse grained, (C) allochthonous, fine grained, (D) local, coarse grained, and (E) local, fine grained. Marine isotope stages (MIS) are shown to the right. Periods of increased contribution of local IRD are highlighted to the far right.

Fig. 10. A. Total IRD concentration >250 µm in number per gram dry weight sediment. B–E.

Relative contribution of the four end-members presented in Fig. 9. F. $\delta^{18}O$ record of Greenland NGRIP ice core (NGRIP Members 2004). Greenland interstadials and Heinrich events are numbered. Peak interstadials are marked by pink bars, Heinrich stadials and other selected cold climate intervals are indicated by blue bars. Marine isotope stages (MIS) are shown to the right. LIA='Little ice age'; YD=Younger Dryas.

Fig. 11. Zoom-in on the period 50–15 ka for cores JM04-025PC (025PC, red) and JM03-374PC (374PC, blue) of (A) flux of IRD, (B) % quartz (indicating influence of local IRD versus allochthonous IRD), and (C) grain-size ratio (interpreted as indicator for influence of icebergs versus sea ice as transport mechanism). Location of Heinrich Events are marked with blue bars and Greenland interstadial and Heinrich events are numbered.

Table 1. Conventional AMS ^{14}C dates, calibrated ages and magnetic susceptibility (MS) Tie-points (in italics).

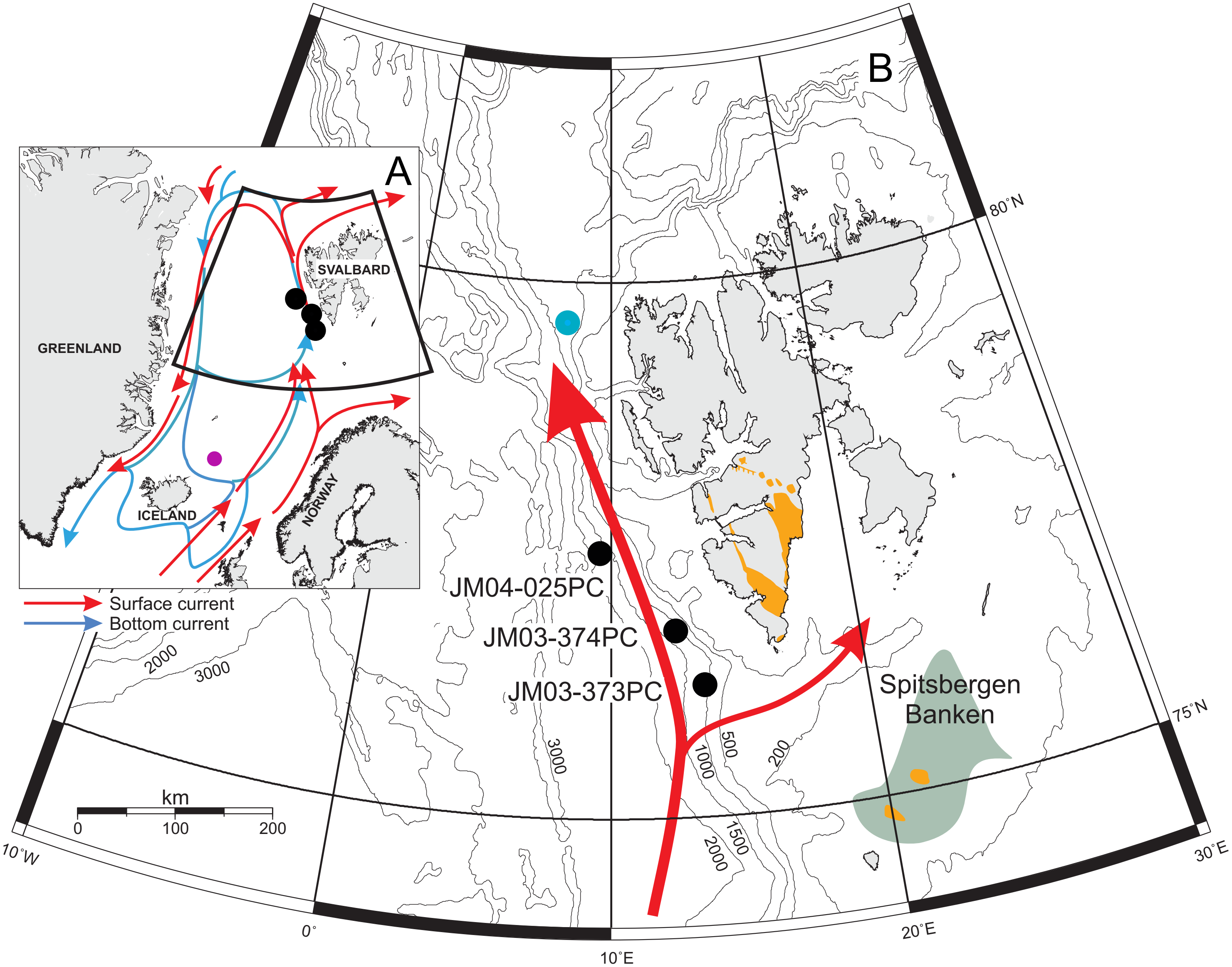

A
GREENLAND
SVALBARD
ICELAND
NORWAY
Surface current
Bottom current
B
80°N
75°N
JM04-025PC
JM03-374PC
JM03-373PC
Spitsbergen
Banken
2000
3000
3000
500
1000
200
1500
2000
km
0
100
200
10°W
0°
10°E
20°E
30°E

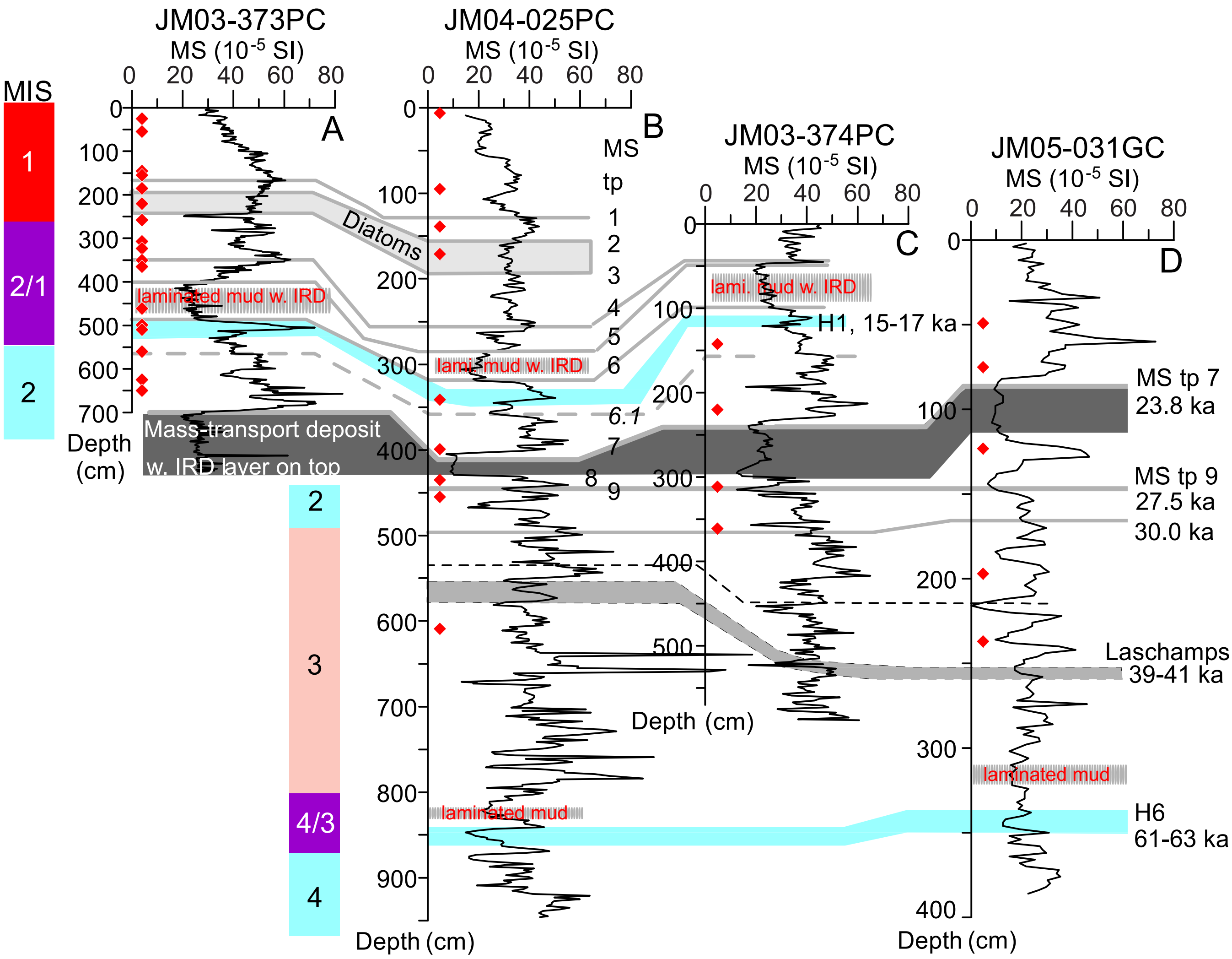

JM03-373PC
MS (10-5 SI)
JM04-025PC
MS (10-5 SI)
JM03-374PC
MS (10-5 SI)
JM05-031GC
MS (10-5 SI)
MIS
1
2/1
2
2
3
4/3
4
A
B
C
D
MS tp
Diatoms
laminated mud w. IRD
lami. mud w. IRD
lami. mud w. IRD
H1, 15-17 ka
MS tp 7
23.8 ka
MS tp 9
27.5 ka
30.0 ka
Laschamps
39-41 ka
laminated mud
laminated mud
H6
61-63 ka
Mass-transport deposit
w. IRD layer on top
6.1
Depth (cm)
Depth (cm)
Depth (cm)
Depth (cm)

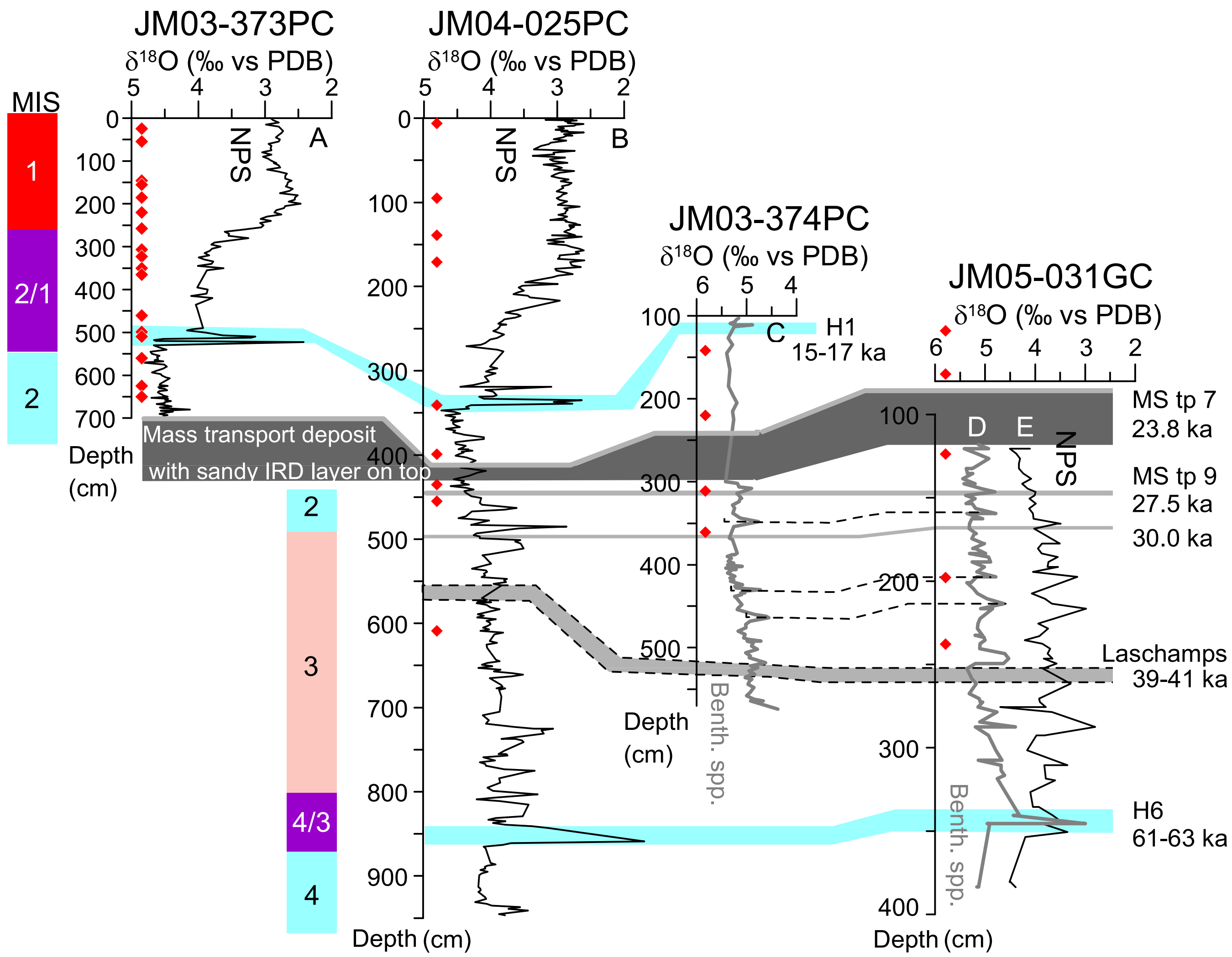

JM03-373PC
δ18O (‰ vs PDB)
JM04-025PC
δ18O (‰ vs PDB)
JM03-374PC
δ18O (‰ vs PDB)
JM05-031GC
δ18O (‰ vs PDB)
MIS
1
2/1
2
3
4/3
4
A
B
C
D
E
NPS
Benth. spp.
Depth (cm)
Mass transport deposit
with sandy IRD layer on top
H1
15-17 ka
MS tp 7
23.8 ka
MS tp 9
27.5 ka
30.0 ka
Laschamps
39-41 ka
H6
61-63 ka

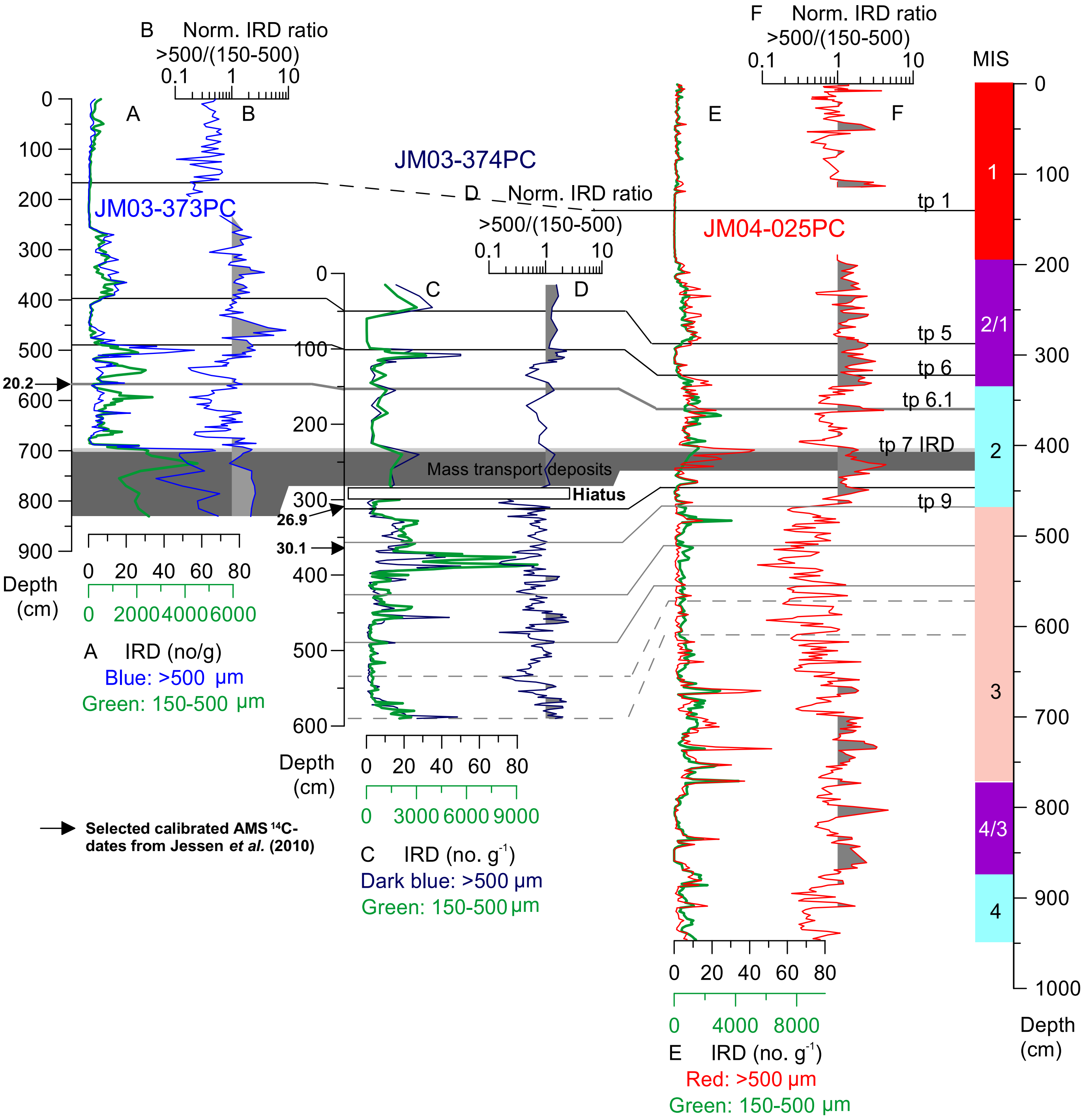

B Norm. IRD ratio
>500/(150-500)
0.1 1 10
A
B
JM03-373PC
JM03-374PC
D Norm. IRD ratio
>500/(150-500)
0.1 1 10
C
D
F Norm. IRD ratio
>500/(150-500)
0.1 1 10
E
F
JM04-025PC
MIS
1
2/1
2
3
4/3
4
tp 1
tp 5
tp 6
tp 6.1
tp 7 IRD
tp 9
Mass transport deposits
Hiatus
20.2
26.9
30.1
Depth (cm)
A IRD (no/g)
Blue: >500 μm
Green: 150-500 μm
C IRD (no. g-1)
Dark blue: >500 μm
Green: 150-500 μm
E IRD (no. g-1)
Red: >500 μm
Green: 150-500 μm
Selected calibrated AMS 14C-dates from Jessen et al. (2010)

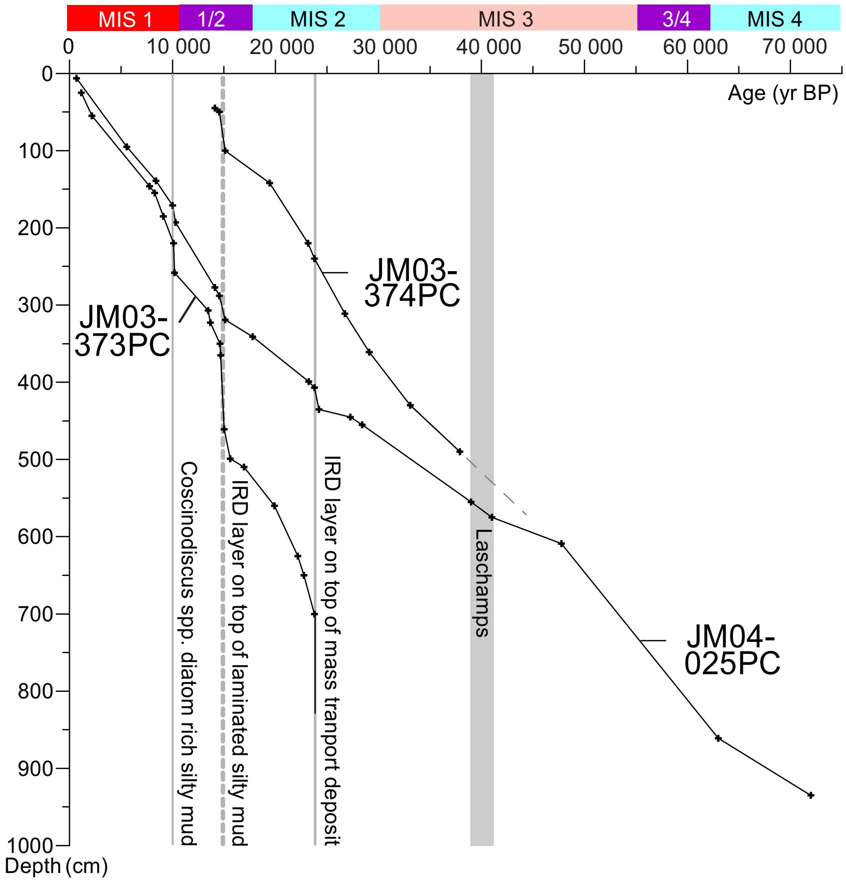

MIS 1
1/2
MIS 2
MIS 3
3/4
MIS 4
0
10 000
20 000
30 000
40 000
50 000
60 000
70 000
Age (yr BP)
0
100
200
300
400
500
600
700
800
900
1000
Depth (cm)
JM03-374PC
JM03-373PC
JM04-025PC
Coscinodiscus spp. diatom rich silty mud
IRD layer on top of laminated silty mud
IRD layer on top of mass tranport deposit
Laschamps

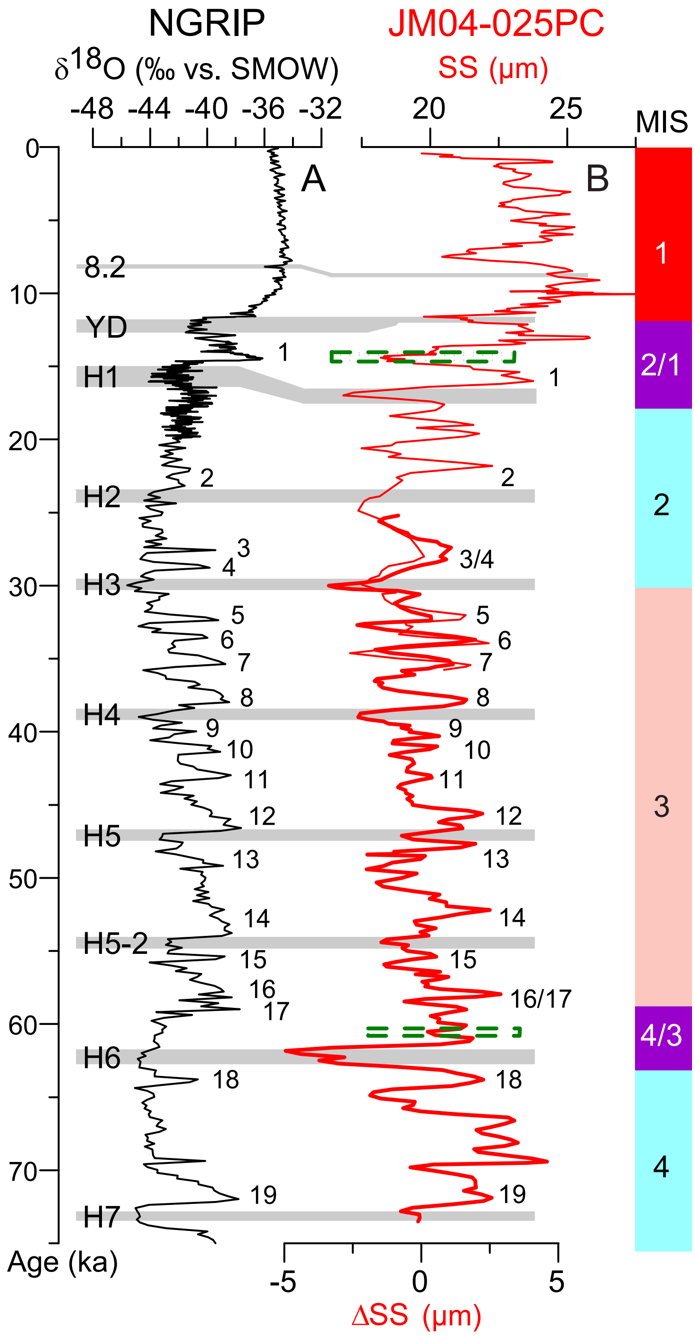

NGRIP
δ18O (‰ vs. SMOW)
-48 -44 -40 -36 -32
JM04-025PC
SS (μm)
20 25
MIS
A
B
8.2
YD
H1
H2
H3
H4
H5
H5-2
H6
H7
1 2 3 4 5 6 7 8 9 10 11 12 13 14 15 16 17 18 19
3/4
16/17
1
2/1
2
3
4/3
4
0 10 20 30 40 50 60 70
Age (ka)
-5 0 5
ΔSS (μm)

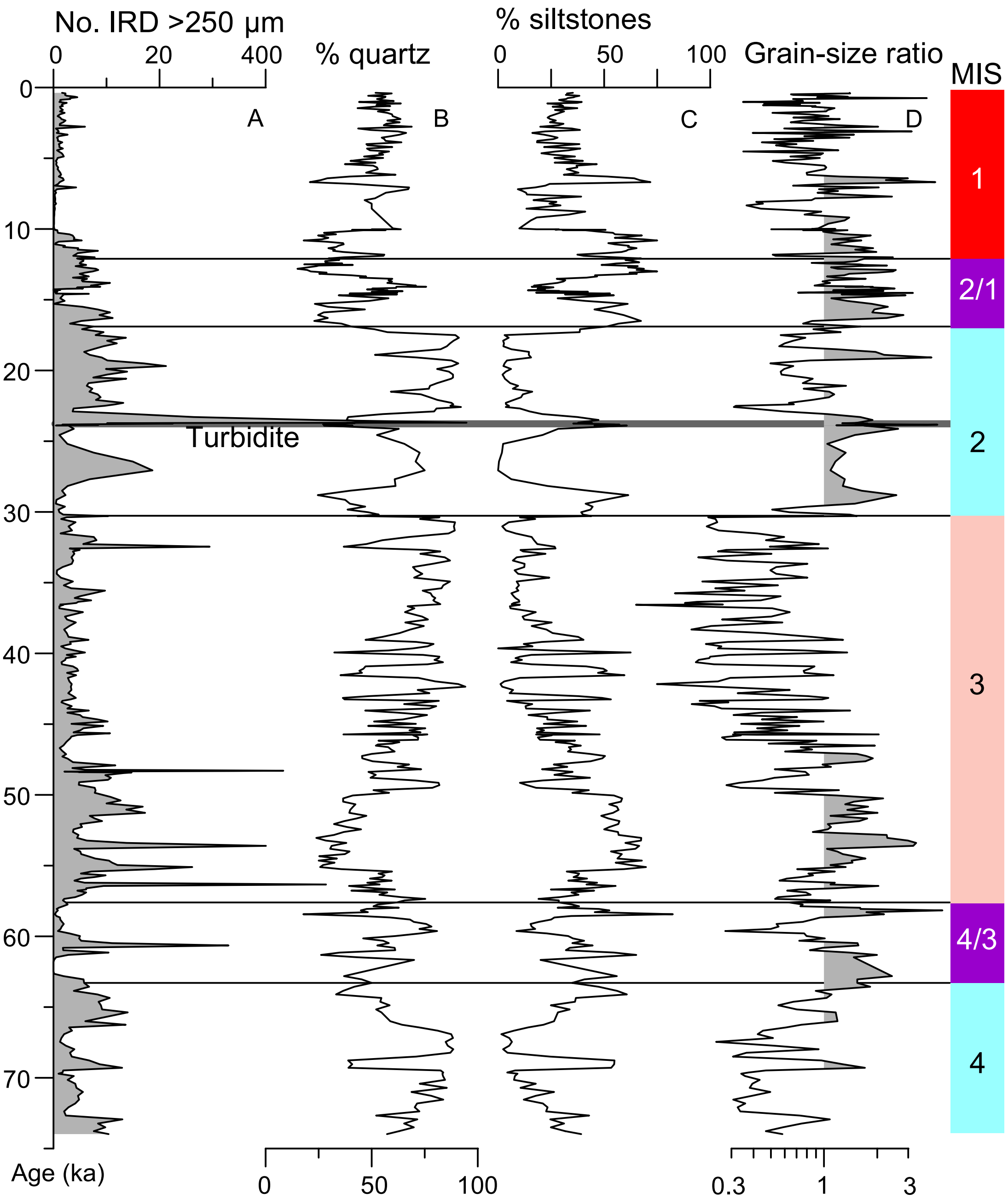
No. IRD >250 µm
0
20
400
A
% quartz
B
% siltstones
0
50
100
C
Grain-size ratio
D
MIS
1
2/1
2
3
4/3
4
Turbidite
0
10
20
30
40
50
60
70
Age (ka)
0
50
100
0.3
1
3

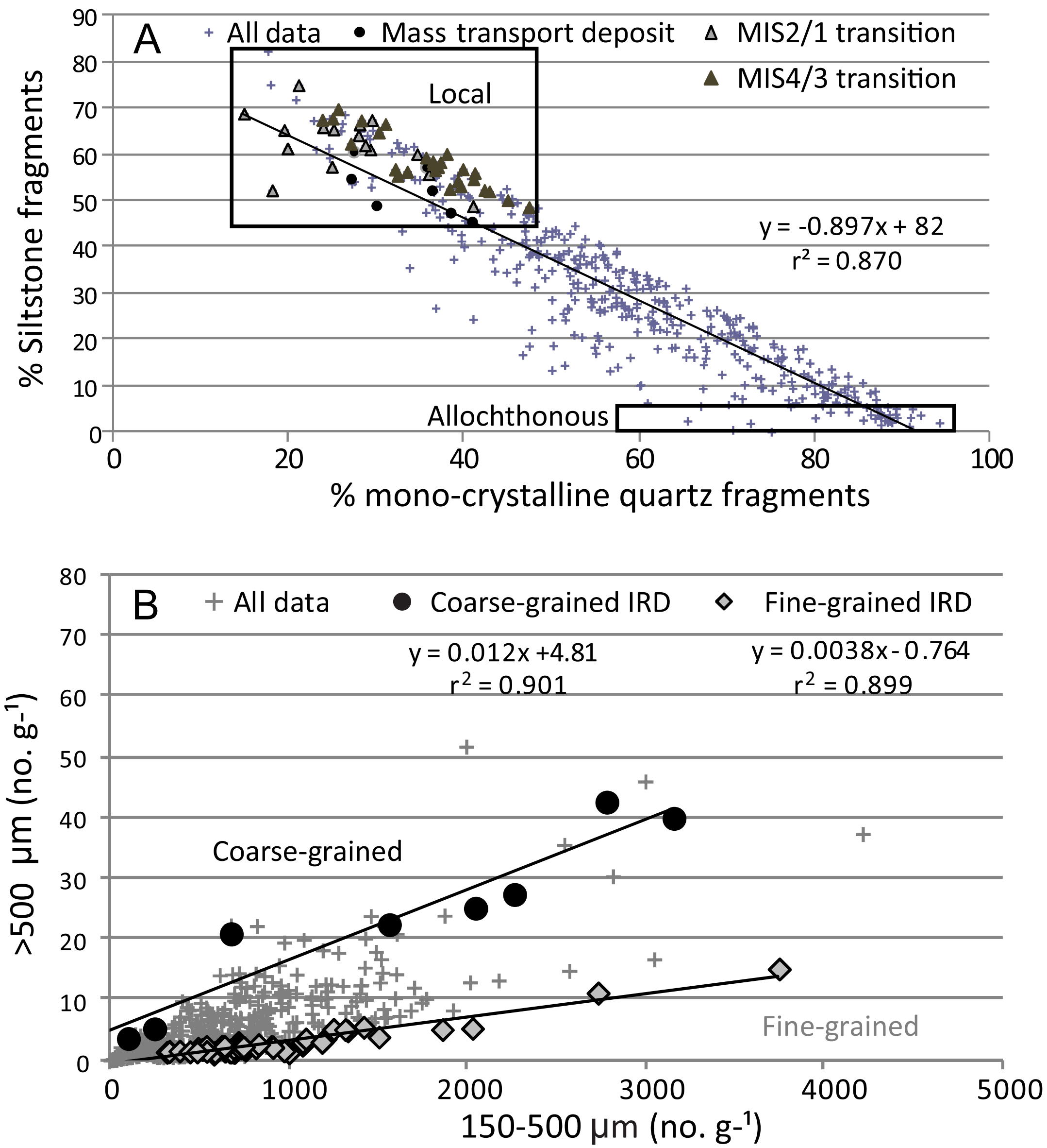

A
All data
Mass transport deposit
MIS2/1 transition
MIS4/3 transition
Local
Allochthonous
y = -0.897x + 82
r² = 0.870
% Siltstone fragments
% mono-crystalline quartz fragments
B
All data
Coarse-grained IRD
Fine-grained IRD
y = 0.012x +4.81
r² = 0.901
y = 0.0038x - 0.764
r² = 0.899
Coarse-grained
Fine-grained
>500 µm (no. g-1)
150-500 µm (no. g-1)

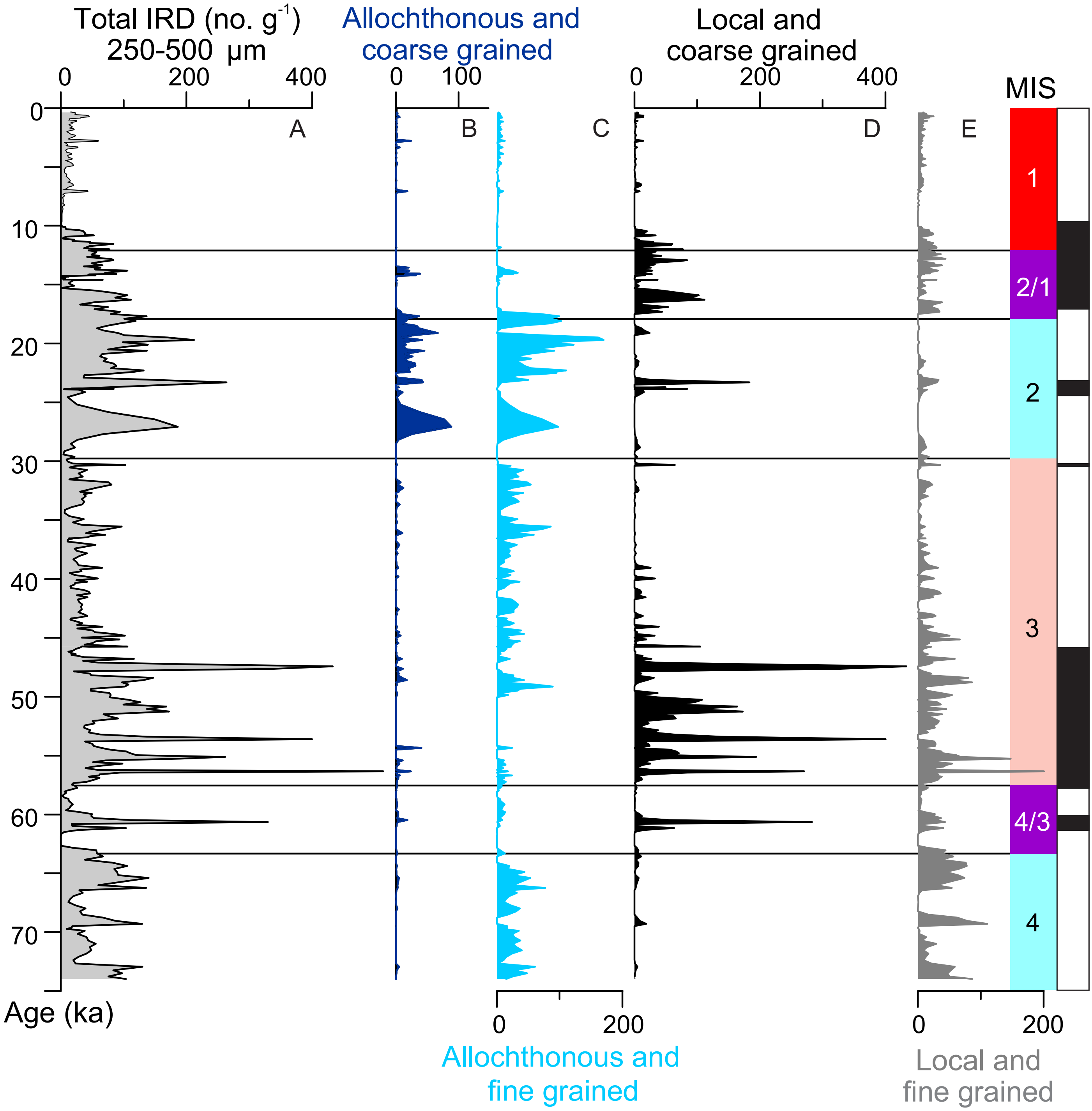

Total IRD (no. g-1)
250-500 μm
0
200
400
Allochthonous and
coarse grained
0
100
Local and
coarse grained
0
200
400
MIS
A
B
C
D
E
1
2/1
2
3
4/3
4
0
10
20
30
40
50
60
70
Age (ka)
0
200
Allochthonous and
fine grained
0
200
Local and
fine grained

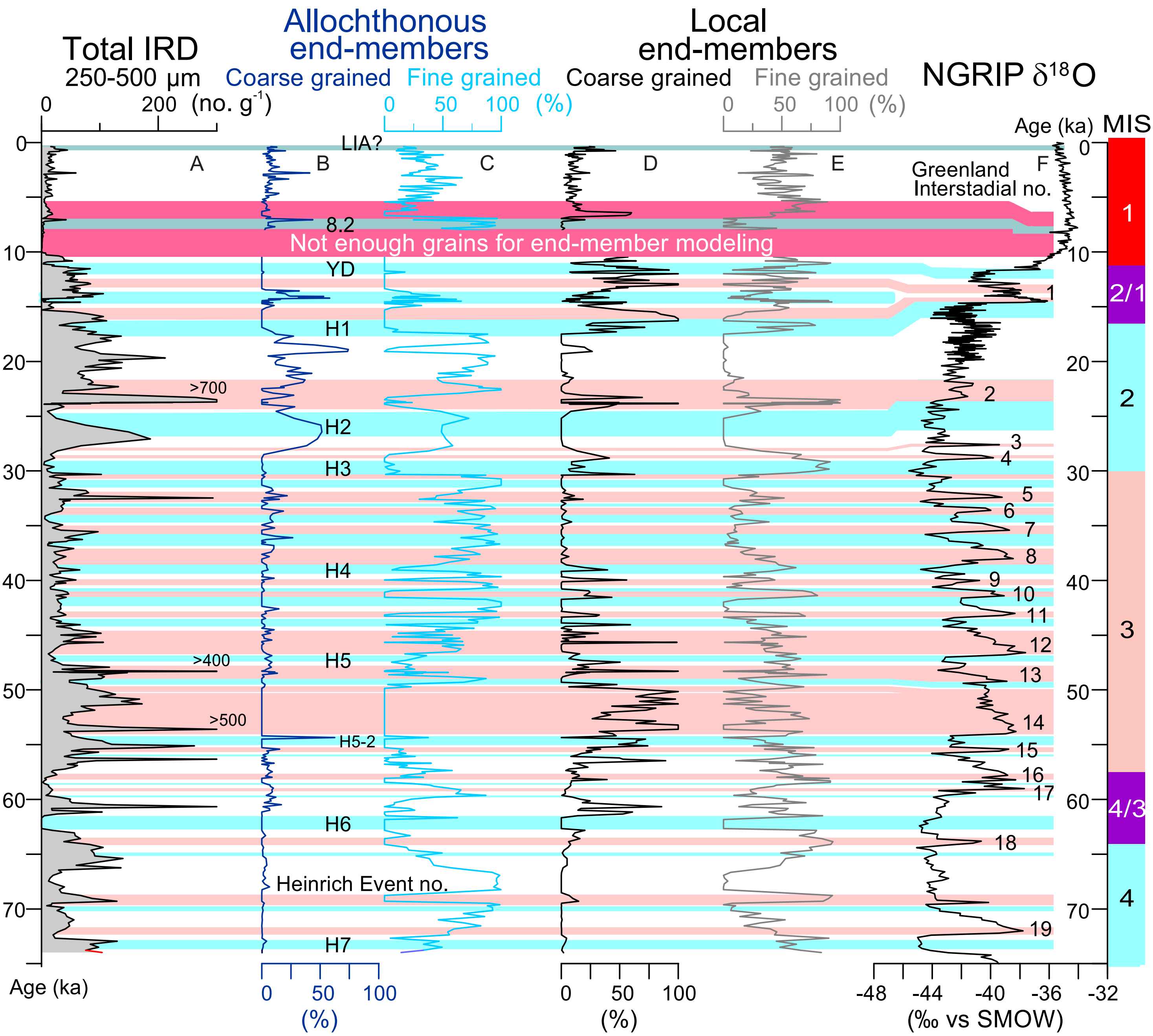

Total IRD
250-500 µm
0 200 (no. g-1)
Allochthonous end-members
Coarse grained
Fine grained
0 50 100 (%)
Local end-members
Coarse grained
Fine grained
0 50 100 (%)
NGRIP δ18O
Age (ka)
MIS
LIA?
A
B
C
D
E
F
Greenland Interstadial no.
8.2
Not enough grains for end-member modeling
YD
H1
H2
H3
H4
H5
H5-2
H6
H7
Heinrich Event no.
>700
>400
>500
1
2
3
4
5
6
7
8
9
10
11
12
13
14
15
16
17
18
19
2/1
4/3
0 10 20 30 40 50 60 70
Age (ka)
0 50 100
(%)
-48 -44 -40 -36 -32
(‰ vs SMOW)

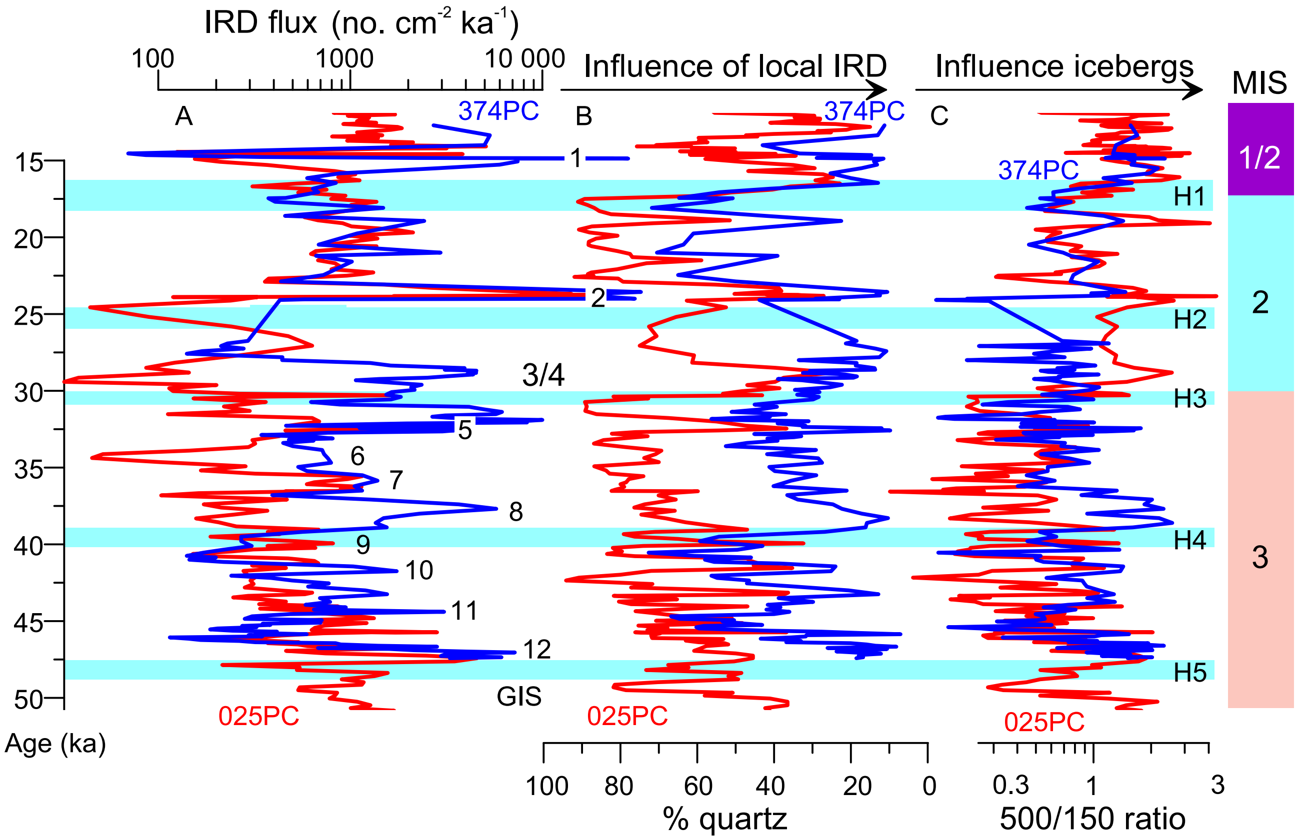

IRD flux (no. cm-2 ka-1)
100
1000
10 000
Influence of local IRD
Influence icebergs
MIS
A
374PC
B
374PC
C
374PC
1/2
2
3
H1
H2
H3
H4
H5
1
2
3/4
5
6
7
8
9
10
11
12
GIS
025PC
025PC
025PC
15
20
25
30
35
40
45
50
Age (ka)
100
80
60
40
20
0
% quartz
0.3
1
3
500/150 ratio

Table 1

Depth (cm)	AMS ^{14}C date	Cal. age (ka)	Lab. Reference	Reference
JM03-373PC				
25	1595 ±40	1155 ±50	AAR-8925	Rasmussen et al., 2007
55	2505 ±40	2175 ±60	AAR-8926	Rasmussen et al., 2007
146	7310 ±45	7775 ±55	AAR-8927	Rasmussen et al., 2007
155	7790 ±60	8255 ±65	AAR-8768	Rasmussen et al., 2007
185	8505 ±60	9134 ±80	AAR-8928	Rasmussen et al., 2007
220	9275 ±65	10,060 ±90	AAR-8796	Rasmussen et al., 2007
258	9355 ±55	10,215 ±75	AAR-10741	Jessen et al,. 2010
307	12,020 ±70	13,485 ±90	AAR-13139	Jessen et al,. 2010
323	12,210 ±100	13,665 ±120	AAR-13140	Jessen et al,. 2010
350	13,310 ±180	14,730 ±425	AAR-8769	Rasmussen et al., 2007
365	12,890 ±110	14,650 ±235	AAR-8918	Rasmussen et al., 2007
461	13,180 ±140	15,200 ±275	Tua-3977	Rasmussen et al., 2007
499	13,450 ±90	15,610 ±160	AAR-8762	Rasmussen et al., 2007
510	14,370 ±100	16,930 ±185	AAR-8770	Rasmussen et al., 2007
560	16,920 ±120	19,960 ±170	AAR-8771	Rasmussen et al., 2007
567	*17,110 ±120*	*20,170 ±170*	*MS Tie-point 6.1*	*This study*
625	18,690 ±120	22,135 ±140	AAR-8772	Rasmussen et al., 2007
650	19,310 ±140	22,780 ±170	AAR-8773	Rasmussen et al., 2007
JM03-374PC				
142	16,520 ±110	19,440 ±160	AAR-8765	Jessen et al,. 2010
152	*17,110 ±120*	*20,170 ±170*	*MS Tie-point 6.1*	*This study*
220	19,630 ±150	23,165 ±205	AAR-8766	Jessen et al,. 2010
311	22,840 ±190	26,900 ±340	AAR-9070	Jessen et al,. 2010
361	25,470 ±250	29,140 ±280	AAR-10624	Jessen et al,. 2010
JM04-025PC				
6.3	1125 ±40	680 ±35	AAR-10851	Jessen et al., 2010
95	5220 ±55	5580 ±65	AAR-10855	Jessen et al., 2010
139	7945 ±50	8400 ±50	AAR-10748	Jessen et al., 2010
171	9215 ±60	10,030 ±100	AAR-11989	Jessen et al., 2010
193	*9390 ±150*	*10,270 ±200*	*MS Tie-point 3*	Jessen et al., 2010
277	*12,590 ±150*	*14,110 ±255*	*MS Tie-point 4*	Jessen et al., 2010
289	*12,840 ±150*	*14,550 ±320*	*MS Tie-point 5*	Jessen et al., 2010
319	*13,140 ±150*	*15,130 ±290*	*MS Tie-point 6*	Jessen et al., 2010
341	15,020 ±90	17,790 ±115	AAR-10852	Jessen et al., 2010
360	*17,110 ±120*	*20170 ±170*	*MS Tie-point 6.1*	*This study*
399	19,670 ±130	23,210 ±135	AAR-10749	Jessen et al., 2010
435	20,570 ±150	24,230 ±180	AAR-10750	Jessen et al., 2010
445	23,340 ±200	27,280 ±190	*MS Tie-point 9*	Jessen et al., 2010
455	24,790 ±210	28,420 ±240	AAR-10856	Jessen et al., 2010
555	Laschamp	39		Snowball et al., 2007
575	Laschamp	41		Snowball et al., 2007
609	44,840 ±1900	47,770 ±1590	AAR-10857	Jessen and Rasmussen, 2015
861	MIS 4/3	63		Jessen and Rasmussen, 2015
935	MIS 4	72		Jessen and Rasmussen, 2015